Frozen-soil hydrological modeling for a mountainous catchment at northeast of the Qinghai-Tibet Plateau

Hongkai Gao 1, 2*, Chuntan Han 3, Rensheng Chen 3, Zijing Feng 2, Kang Wang 1,2, Fabrizio Fenicia 4, Hubert Savenije 5

1 Key Laboratory of Geographic Information Science (Ministry of Education of China), East China Normal University, Shanghai, China

2 School of Geographical Sciences, East China Normal University, Shanghai, China

3 Qilian Alpine Ecology and Hydrology Research Station, Key Lab. of Ecohydrology of Inland River Basin, Northwest Institute of Eco-Environment and Resources, Chinese Academy of Sciences, Lanzhou 730000, China

4 Eawag, Swiss Federal Institute of Aquatic Science and Technology, Dubendorf, Switzerland

5 Delft University of Technology, Delft, the Netherlands

*Corresponding to: Hongkai Gao (hkgao@geo.ecnu.edu.cn)

Abstract:

Increased attention directed at frozen-soil hydrology has been prompted by climate change. In spite of an increasing number of field measurements and modeling studies, the impact of frozen-soil on hydrological processes at the catchment scale is still unclear. However, frozen-soil hydrology models have mostly been developed based on a "bottom-up" approach, i.e. by aggregating prior knowledge at pixel scale, which is an approach notoriously suffering from equifinality and data scarcity. Therefore, in this study, we explore the impact of frozen-soil at catchment-scale, following a "top-down" approach, implying: expert-driven data analysis → qualitative perceptual model → quantitative conceptual model → testing of model realism. The complex mountainous Hulu catchment, northeast of the Qinghai-Tibet Plateau (QTP), was selected as the study site. Firstly, we diagnosed the impact of frozen-soil on catchment hydrology, based on multi-source field observations, model discrepancy, and our expert knowledge. Two new typical hydrograph properties were identified: the low runoff in the early thawing season (LRET) and the discontinuous baseflow recession (DBR). Secondly, we developed a perceptual frozen-soil hydrological model, to explain the LRET and DBR properties. Thirdly, based on the perceptual model and a landscape-based modeling framework (FLEX-Topo), a semi-distributed conceptual frozen-soil hydrological model (FLEX-Topo-FS) was developed. The results demonstrate that the FLEX-Topo-FS model can represent the effect of soil freeze/thaw processes on hydrologic

36 connectivity and groundwater discharge and significantly improve hydrograph simulation,
37 including the LRET and DBR events. Furthermore, its realism was confirmed by alternative
38 multi-source and multi-scale observations, particularly the freezing and thawing front in the
39 soil, the lower limit of permafrost, and the trends in groundwater level variation. To the best
40 of our knowledge, this study is the first report of LRET and DBR processes in a mountainous
41 frozen-soil catchment. The FLEX-Topo-FS model is a novel conceptual frozen-soil
42 hydrological model, which represents these complex processes and has potential for wider
43 use in the vast QTP ~~Tibetan Plateau~~ and other cold mountainous regions.

44

1 Introduction

1.1 Frozen-soil hydrology: one of twenty-three unsolved problems

47 The Qinghai-Tibet~~an~~ Plateau (QTP) is largely covered by frozen soil and is characterized by
48 a fragile cold and arid ecosystem (Immerzeel et al., 2010; Ding et al., 2020). As this region
49 serves as the "water tower" for nearly 1.4 billion people, understanding the frozen soil
50 hydrology is important for regional and downstream water resources management and
51 ecosystem conservation. Frozen soil prevents vertical water flow which often leads to
52 saturated soil conditions in continuous permafrost, while confining subsurface flow through
53 perennially unfrozen zones in discontinuous permafrost (Walvoord and Kurylyk, 2016). As an
54 aquiclude layer, frozen soil substantially controls surface runoff and its hydraulic connection
55 with groundwater. The freeze–thaw cycle in the active layer significantly impacts soil water
56 movement direction, velocity, storage capacity, and hydraulic conductivity (Bui et al., 2020;
57 Gao et al., 2021).

58 Frozen-soil hydrology attracts increasing attention, as the cold regions, e.g. QTP~~Tibetan~~
59 ~~Plateau~~ and Arctic, are undergoing rapid changes (Song et al., 2020; Tananaev et al., 2020).
60 Frozen-soil thawing also poses great threats to the release of frozen carbon in both high
61 altitude and latitude regions, which is likely to create substantial impacts on the climate
62 system (Wang et al., 2020). Attention is also growing for the impact of frozen-soil hydrology
63 on nutrient transport and organic matter, and frozen soil–climate feedback (Tananaev et al.,
64 2020). Hence, there are strong motivations to better understand frozen-soil hydrological
65 processes (Bring et al., 2016).

66 Frozen-soil degradation and its impact on hydrology is one of the research frontiers for the
67 hydrologic community (Blöschl et al., 2019; Zhao et al., 2020; Ding et al., 2020). "How will
68 cold region runoff and groundwater change in a warmer climate?" was identified by the
69 International Association of Hydrological Sciences (IAHS), as one of the 23 major unsolved
70 scientific problems (Blöschl et al., 2019), which requires stronger harmonization of
71 community efforts.

1.2 The frontier of frozen-soil hydrology

Knowledge on frozen-soil hydrology was acquired through detailed investigations at isolated locations over various time spans by hydrologists and geocryologists (Woo et al., 2012; Gao et al., 2021). At the core scale, there are many measurements of soil profiles, including but not limited to soil temperature (Kurylyk et al., 2016; Han et al., 2018), soil moisture (Dobinski, 2011; Chang et al., 2015), groundwater fluctuation (Ma et al., 2017; Chiasson-Poirier et al., 2020), and active layer seasonal freeze-thaw processes (Wang et al., 2016; Farquharson et al., 2019). At the plot/hillslope scale, land surface energy and water fluxes are measured by eddy covariance, large aperture scintillometer (LAS), lysimeter, and multi-layers meteorological measurements. Geophysical detection technology allows us to measure various subsurface permafrost features. At the basin scale, except for traditional water level and runoff gauging, water sampling and the measurements of isotopes and chemistry components provide important complementary data to understand catchment scale hydrological processes (Streletskiy et al., 2015; Ma et al., 2017; Yang et al., 2019). Remote sensing technology, including optical, near- and thermal-infrared, passive and active microwave remote sensing, has been used to identify surface landscape features (e.g. vegetation and snow cover) and directly or indirectly retrieve subsurface variables (e.g. near-surface soil freeze/thaw and permafrost state) in frozen-soil regions (Nitze et al., 2018; Jiang et al., 2020).

Besides measurement, modeling provides another indispensable dimension to understand frozen-soil hydrology in an integrated way, and make predictions in climate change. There has been a revival in the development of frozen-soil hydrological models simulating coupled heat and water transfer. Such physically-based models typically calculate seasonal freeze–thaw through solving heat transfer equations. Such equations are either solved analytically or numerically (Walvoord and Kurylyk, 2016). The Stefan equation is a typical example of the analytical approach, which calculates the depth from the ground surface to the thawing (freezing) horizon by the integral of ground surface temperature and soil features. The Stefan equation is widely used to estimate active layer thickness (Zhang et al., 2005; Xie and Gough, 2013), and is incorporated into some hydrological models (Wang L, 2010; Fabre et al. 2017). The numerical solution schemes (e.g., finite difference, finite element, or finite volume) to model ground freezing and thawing, is typically applied to one-dimensional infiltration into frozen soils, and is included in models such as SHAW (Liu et al. 2013), CoupModel (Zhou et al., 2013), the distributed water-heat coupled (DWHC) model (Chen et al. 2018), the distributed ecohydrological model (GBEHM) (Wang Y. 2018), and the three-dimensional SUTRA model (Evans et al. 2018). Andresen et al (2020) compared 8 permafrost models on soil moisture and hydrology projection across the major Arctic river basins, and found that ~~most models project a long-term drying of surface soil, but~~ the projection vari~~ed~~ed strongly in magnitude and spatial pattern. Except for hydrological models, many land surface models explicitly consider the freeze-thaw process, in order to improve land surface water and energy budget estimation and weather forecasting accuracy in frozen-soil areas. Such models include VIC (Cuo et al., 2015), JULES (Chadburn et al., 2015), CLM (Niu et al., 2006; Oleson et al., 2013; Gao et al., 2019), CoLM (Xiao et al., 2013),

114   Noah-MP (Li et al., 2020), ORCHIDEE (Gouttevin et al., 2012). Comprehensive reviews on
115   frozen-soil hydrological models can be found in Walwoord and Kurylyk (2016), Jiang et al.
116   (2020), and Gao et al. (2021).

1.3 The challenge of frozen-soil hydrological modeling

118   Although numerous frozen-soil hydrological models were developed, most models have
119   strong prior assumptions on the impacts of frozen-soil on hydrological behavior (Walvoord
120   and Kurylyk, 2016; Gao et al., 2021). Such models follow a "bottom-up" modeling approach,
121   which presents an "upward" or "reductionist" philosophy, based on the aggregation of
122   small-scale processes and *a priori* perceptions (Jarvis, 1993; Sivapalan et al., 2003). However,
123   most of the "upward" process understanding has been obtained from in-situ observation
124   and in-situ modeling, which have limited spatial and invariably limited temporal coverage
125   (Brutsaert, and Hiyama, 2012). It is worthwhile to note that frozen-soil has tremendous
126   spatial-temporal heterogeneities, which are strongly influenced by many intertwined factors,
127   including but not limited to climate, topography, geology, soil texture, snow cover, and
128   vegetation. Upscaling could average out some variables, and turn other variables visible and
129   even become dominant processes (Fenicia and McDonnell, 2022). Unfortunately, translating
130   spot/hillslope scale frozen-soil process to its influence on catchment scale hydrology,
131   guided by carefully expert analysis, and constrained by multi-source measurements, is still
132   largely unexplored.

133   The effects of the soil freeze/thaw process on hydrology at catchment scale is still
134   inconclusive. In the headwaters of the Yellow River, some modeling studies concluded that
135   permafrost has significant impact on streamflow (Sun et al., 2020). But in Sweden and the
136   northeast of the United States, other studies found frozen soil have negligible impact on
137   streamflow (Shanley and Chalmers, 1999; Lindstrom et al., 2002). Some studies found that
138   the impact of frozen soil on streamflow is concentrated in certain periods. For example,
139   Osuch et al. (2019) found permafrost to impact on groundwater recession and storage
140   capacity of the active layer in ~~Svalbard island~~Svalbard Island; Nyberg et al. (2001) found that
141   in the Vindeln Research Forest in northern Sweden permafrost impacted streamflow only in
142   springs. Hence, we argue that the impact of local scale freeze-thaw process on runoff
143   should be regarded as a hypothesis to be verified or rejected.

144   The unexplored frozen-soil hydrology is especially true for mountainous Asia, due to the
145   lack of long-term observations as a result of the difficulty of access and high cost of
146   operation. The cold region of the ~~Tibetan Plateau~~QTP is characterized by relatively thin and
147   warm frozen-soil with low ice content, due to the unique environmental conditions, arid
148   climate, high elevation and steep geothermal gradient (Cao et al., 2019; Zhao et al., 2020;
149   Jiang et al., 2020). Snow cover is thinner, and vegetation cover is poorer than in Arctic
150   regions. These features limit the insulation effect on freeze-thaw processes, resulting in a
151   much larger active layer depth (Pan et al., 2016). Topographical features, including elevation
152   and aspect, are major factors affecting permafrost distribution. The complex mountainous
153   terrain, as a result of recent tectonic movement, leads to large spatial heterogeneity in the
154   energy and water balance, and underexplored frozen-soil hydrology on the ~~Tibetan Plateau~~

155 QTP (Gao et al., 2021).

1.4 Aims and scope

157 In this study, we utilized a "top-down" approach (Sivapalan et al., 2003), to understand the
158 effect of frozen-soil on hydrology in the Hulu catchment on the northeastern edge of the
159 QTPTibetan Plateau. The aims of this study are as below:

160 1) Diagnosing the impacts of frozen-soil on hydrology in the mountainous Hulu
161   catchment, with multi-source, multi-scale data and model discrepancy;

162 2) Developing a quantitative conceptual frozen-soil hydrological model, based on expert-
163   driven interpretation in the form of perceptual model for the Hulu catchment;

164 3) Testing the realism of the conceptual frozen-soil hydrological model, with multi-source
165   and multi-scale observations.

166 In this paper, we firstly introduced the study site and data in Section 2; an expert-driven
167 perceptual frozen-soil hydrology model was proposed in Section 3; a semi-distributed
168 conceptual frozen-soil hydrological model, FLEX-Topo-FS, was developed in Section 4; the
169 realism of the FLEX-Topo-FS model was tested in Section 5; in Section 6 and 7, last but not
170 least, we made discussions and draw the conclusions.

2 Study site and data

172 The Hulu catchment (38°12´–38°17´ N, 99°50´–99°54´E) is located in the upper reaches of
173 the Heihe River basin, the northeast edge of the Tibetan PlateauQTP in northwest China
174 (Figure 1). The elevation ranges from– 2960 to 4820 m a.s.l., gradually increasing from
175 north to south (Figure 1) (Chen et al., 2014; Han et al., 2018). Most precipitation occurs in
176 the summer monsoon time, and snowfall in winter is limited (Han et al., 2018; Jiang et al.,
177 2020). There is a runoff gauging station at the outlet, controlling an area of 23.1 km^2. Two
178 minor tributaries are sourced from glaciers (east) and moraine–talus (west) zones, which
179 merge at the catchment outlet. The Hulu catchment has rugged terrain and very little
180 human disturbance. We identified four main landscape types, i.e. glaciers (5.6%), alpine
181 desert (53.5%), vegetation hillslope (37.5%), and riparian zone (3.4%) (Figure 2).

182 The Hulu catchment mostly extends on seasonal frozen-soil and permafrost (Zou et al.,
183 2014; Ma et al., 2021). Field survey in the upper Heihe revealed that the lower limit of
184 permafrost was 3650m~3700m (Wang et al., 2013), above that elevation is permafrost, and
185 below is seasonal frozen-soil. In the Hulu catchment, the lower limit of permafrost is around
186 3650m (Figure 1). Permafrost covers 64% of the catchment area, and the seasonal frozen-
187 soil covers 36%. There is a strong co-existence between soil freeze-thaw feature and
188 landscapes (Figure 1). Permafrost and moraine/talus with poor vegetation cover co-exist in
189 higher elevation, with large heat conductivity and less heat insulation in winter, resulting
190 deep frozen depth. The seasonal frozen soil in relative lower elevation has better vegetation
191 cover, with better heat insulation and less heat conductivity in winter, resulting in shallower

192 frozen depth.

193 The elevation of the hydrometeorological gauging station is 2980m. We collected daily
194 runoff, daily average 2m air temperature, and daily precipitation from January 1st 2011 to
195 December 31st 2014. There was a flood event in 2013, which damaged the water level
196 sensor, resulted in a runoff data gap from June 17th to July 10th in 2013. Soil moisture was
197 measured in 20cm, 40cm, 80cm, 120cm, 180cm, 240cm, and 300cm depths from October 1st
198 2011 to December 31st 2013, with a data gap between August 3rd 2012 and October 2nd
199 2012. In the same soil moisture site, we also observed the soil freeze/thaw depth from 2011
200 to 2014. Groundwater depth was measured at WW01 site by four wells, with depth of 5m,
201 10m, 15m, and 25m respectively (Pan et al., 2021). The observation period was from 2016 to
202 2019, not overlaid with other hydrometeorological variables. Hence, we merely used the
203 groundwater level to qualitatively constrain and test our perceptual model.

3 An expert-driven perceptual frozen-soil hydrology model

204

based on field observations

205

206 Perceptual model is increasingly recognized as the central importance in hydrological
207 model development (Fenicia and McDonnell, 2022). Although perceptual model is a
208 qualitative representation of hydrological system, it bridges the gap between
209 experimentalists and modelers, and hold the base for quantitative conceptual model. In this
210 study, we developed a perceptual frozen-soil hydrology model for the Hulu catchment,
211 based on field measurements and our expertise.

3.1 Observation1: Low runoff in the early thawing season (LRET)

212

213 Precipitation-runoff time series analysis is a tradition and powerful tool to understand
214 catchment hydrology. When we plot Hulu catchment's precipitation and runoff data
215 together, we observed an interesting phenomenon, i.e. low runoff in the early thawing
216 season (LRET) phenomenon (Figure 3). For example, on June 5-9, 2013, there was a 45.7mm
217 rainfall event, with air temperature ranging from 3.0℃ to 11.9℃, but with only 0.68mm in
218 total runoff generation. Ma et al., (2021) also showed that in the warm middle June 2015 in
219 Hulu catchment, there was a large rainfall event (over 30mm/d), but no runoff response was
220 observed. Moreover, this LRET phenomenon repeatedly happens every year, which allows
221 us to exclude the possibility of measurement errors.

222 To further investigate the LRET phenomenon, we plot the time series of observed daily
223 precipitation, temperature, runoff, freeze/thaw front depth, and soil moisture profile (20cm,
224 120cm, and 240cm) together (Figure 3). Soil moisture data showed that top soil was dry at
225 the beginning of thawing season. Gradually, soil was thawing from both topsoil and
226 downwards (Figure 3), and simultaneously the soil moisture was increased also downwards.
227 Although the topsoil was thawed, there was still frozen-soil underneath (Figure 3). The

228   water above the frozen-soil layer was even saturated with ponding but no percolation and
229   runoff generation. Moreover, the groundwater level further declined (Figure 1~~1~~2). This
230   illustrated that, during this period, the soil and groundwater system were disconnected, very
231   likely because the frozen soil blocked the percolation. As revealed by isotope data in the
232   Hulu catchment, groundwater contributed the dominant streamflow, i.e. 95% during the
233   frozen period (Ma et al., 2021). Thus, during this process, there was almost no runoff
234   generation, and the only contribution to streamflow during this period was the discharge
235   from groundwater system as baseflow. Our field work experience also verified that in the
236   early thawing season, vehicles were easy to be trapped in mires, because the surface soil
237   was muddy, saturated even over-saturated with ponding. When frozen-soil was completely
238   thawed in summer, trafficability became much better.

239   When completely thawed, the bidirectional thaw fronts meet, the soil moisture in the
240   bottom of frozen soil (around 2.4m in this study site, Figure 3) was increased sharply, and
241   then decreased, with a short period pulse. We also noted that the observation sites of
242   freeze/thaw front depth and soil moisture were both near the outlet of the Hulu catchment
243   in lower elevation (Figure 1). This means once the frozen soil in lower elevation was thawed,
244   soil and groundwater systems were reconnected. Hydrological processes, including
245   groundwater percolation and runoff generation, became the same as ~~normal~~ free of frozen-
246   soil normal circumstances.

Learning from paired catchments

247

248   The LRET phenomenon was widely documented in other cold regions (Figure 4), including
249   but not limited to the headwater of Yellow River (Yang et al., 2019), and ~~the~~ a small
250   headwater catchment at Cape Bounty Arctic Watershed Observatory, Melville Island, NU in
251   Canada (Lafrenière and Lamoureux, 2019). For example, at the headwater of Yellow River,
252   on July 8-9 2014, there was a 21.9mm rainfall event with temperature of 6.5℃, but little
253   1.5m^3/s runoff; and on July 21-23 2014, there was a 27.4mm rainfall event with temperature
254   of 7.2℃, but only 5.1m^3/s runoff. Lafrenière and Lamoureux (2019) found that the
255   undisturbed frozen soil at Cape Bounty Arctic Watershed Observatory had little runoff
256   generation in the early thawing season. But after the frozen-soil was disturbed, the runoff
257   response to rainfall event was much larger. Hence this paired catchment study illustrated
258   that frozen soil played a key role causing the LRET phenomenon.

259   ## 3.2 Observation2: Discontinuous baseflow recession (DBR)

260   Baseflow recession provides an important source of information to infer groundwater
261   characteristic, including its storage properties, subsurface hydraulics, and concentration
262   times (Brutsaert and Sugita, 2008; Fenicia et al., 2006), which is especially true for basins with
263   frozen-soil (Ye et al., 2009; Song et al., 2020~~Gao et al., 2021~~).

264   Baseflow analysis is based on the water balance equation (Equation 1), and linear reservoir
265   assumption (Equation 2). It should be noted that Equation 1 assumes no additional inflows
266   (recharge or thawing) or outflow (capillary rise or freezing). If a reservoir is linear, this
267   implies that the reservoir discharge (Q) has a linear relationship with its storage (S). K_s (days)

268   is time-constant controlling the speed of recession in the linear reservoir. With a larger K_s
269   value, the reservoir empties slower, and vice-versa. Combining Equation 1 and 2, we can
270   derive equation 3, illustrating how discharge depends on time (t), proportional to the initial
271   discharge (Q_0).

272    $$\frac{dS}{dt} = -Q \quad (1)$$

273    $$Q = S/K_s \quad (2)$$

274    $$Q = Q_0 \cdot e^{-t/Ks} \quad (3)$$

Baseflow recession analysis results

276   In Figure 5, we plot the groundwater recession on semi-logarithmic scale. In the beginning
277   of freezing season, baseflow presented a clear linear recession, and was able to be fitted by
278   setting the recession coefficient (K_s) as 80 days. However, interestingly, simultaneously with
279   the LRET phenomenon, we observed a clear discontinuous baseflow recession in the Hulu
280   catchment (Figure 5). The baseflow bended down, and K_s became 60 days in the end of
281   recession periods. This DBR phenomenon informed us that the groundwater system ~~had~~
282   ~~additional outflow, and the groundwater storage~~ was disturbed. We also noted the spikes
283   during the thawing in Fig. 5, which means groundwater was suddenly released. To our best
284   knowledge, these discontinuous baseflow recession (DBR) phenomenon is a new
285   observation for mountainous frozen-soil hydrology.

286   We also plot the variation of groundwater depth of 4 wells at WW01 site from 2016 to 2019
287   (Figure 1, 1~~1~~2). The wells of 5m, 10m, and 15m only had liquid water in thawing seasons,
288   and gradually went dry in recession periods. The water level of the 25m well was decreasing
289   in the entire frozen seasons, but in a discontinuous way. From the observed groundwater
290   depth, the groundwater level decreases faster at beginning. And after the groundwater level
291   dropped below around 17m, the decrease of groundwater level became slower. The turning
292   point from K_s=80d to K_s =60d occurred simultaneously while the groundwater level went
293   down to 17m (Figure 5, 1~~1~~2). The bending down discontinuous baseflow recession and
294   slower decrease of groundwater level indicated that there was a disturbance reduced the
295   groundwater discharge and lead to a slower decrease of groundwater level.

Learning from paired catchments

297   Frozen-soil process is able to disturb the groundwater system, by freezing the liquid
298   groundwater to reduce groundwater storage, and leading to the DBR. But the DBR could
299   also be caused by many other reasons, for instance soil evaporation, root tapping, capillary
300   rise, impermeable layer, and heterogenous hydraulic conductivities in different landscapes
301   (riparian area and hillslope). Since the DBR phenomenon started from the middle of freezing
302   period, and lasted until the end of frozen season, in which time the evaporation, root
303   tapping, and capillary rise were very inactive even totally stopped, which allows us to
304   exclude these impacts. The impermeable layer and heterogenous hydraulic conductivities
305   are both able to result in discontinuous recession in small scale.

306   To further understand the DBR phenomenon, we collected larger scale runoff data in this

307 region, including the Zhamashike (5526 km^2) and Qilian (2924 km^2), which are also the sub-
308 basins of the upper Heihe. The permafrost and seasonal frozen-soil map of the upper Heihe
309 River basin shows that: the Zhamashike sub-basin has 74% permafrost and 26% seasonal
310 frozen soil, which is similar to the Hulu catchment; while the Qilian sub-basin has much less
311 permafrost area (38%), and is mostly covered by seasonal frozen-soil (62%) (Figure 1).

312 Interestingly, when plotting the hydrographs of these two sub-basins on logarithmic scale,
313 we can clearly see that in the permafrost dominated Zhamashike sub-basin discontinuous
314 recessions occurred, with K_s=60d in the early and K_s = 20d in in the end of the recession
315 period. This DBR phenomenon is the same as we found in the Hulu catchment, although the
316 Zhamashike and Hulu catchment have quite different scales (5526 km^2 versus 23.1 km^2)
317 (Chen et al. 2018, Gao et al., 2014). Discontinuous baseflow recession happened almost
318 every year at the Zhamashike station, and we only highlight the hydrograph in 1974 to
319 demonstrate this phenomenon in Figure 6. On the other hand, of similar size as the
320 Zhamashike, the Qilian sub-basin (2924 km^2), which is mostly covered by seasonal frozen-
321 soil, only has one continuous recession, with K_s = 60d. The results from these two paired
322 catchments provided good reasons to interpret the DBR phenomenon in the Hulu
323 catchment as the result of frozen-soil.

324 ## 3.3 Perceptual frozen-soil hydrology model of Hulu catchment

325 We did an expert-driven data analysis of the LRET and DBR observations, including time
326 series analysis of precipitation-runoff, soil moisture profile, freeze/thaw depth, and paired
327 catchments comparison. These comprehensive data analyses allowed us to identify that
328 both the LRET and the DBR were the results of frozen-soil, and motivated the following
329 perceptual model (Figure 7).

330 In the freezing season, at local scale, frozen soil occurs from the top soil downwards. But at
331 catchment scale, the freezing process does not occur in a homogeneous way. Since the
332 higher elevation is colder than the lower elevation, the freezing process starts from higher
333 elevation and downwards. At the beginning of the freezing season, although the top soil is
334 already frozen, the groundwater discharge from the supra-permafrost layer still continues. It
335 was found that the groundwater recession from the supra-permafrost layer determines the
336 dominant part of baseflow in permafrost regions (Brutsaert and Sugita, 2008; Ma et al.,
337 2021). Thus, the baseflow recession contributed by both permafrost and seasonal frozen-
338 soil areas, during this period, appears not to be influenced by frozen topsoil, and maintains
339 a linear recession pattern, with K_s=80d in the Hulu catchment. With the increase of frozen
340 depth, groundwater in the supra-permafrost layer is frozen gradually from higher to lower
341 elevation, which would gradually and dramatically reduce groundwater discharge.

342 In the frozen season, the hydrological processes in the topsoil are almost completely
343 blocked, although there is still very small amount of unfrozen liquid water in the frozen soil.
344 Thus, surface hydrological processes are almost stopped. With the increase of frozen depth,
345 groundwater in the supra-permafrost layer is frozen gradually from higher to lower
346 elevation, which would gradually and but dramatically reduces groundwater discharge.

347 Interestingly, permafrost and seasonal frozen-soil have different impacts on baseflow
348 recession. In seasonal frozen-soil region, with shallower frozen depth, the groundwater is
349 still active, and continues the discharge. But in the permafrost region, the groundwater in
350 the supra-permafrost layer is largely inactive. This means the recession, in the frozen
351 periods, was only contributed by the seasonal frozen-soil area, with faster decline of
352 baseflow, and the bend down of hydrograph, with K_s decreased to 60 days in Hulu
353 catchment. ~~while in the permafrost region, the groundwater in the supra- permafrost layer is~~
354 ~~largely inactive. But because there is still unfrozen liquid water in the frozen soil (Figure 3),~~
355 ~~the model should also allow a small amount of liquid water to exist.~~

356 During the early thawing season, after a long groundwater recession, the groundwater level
357 is deep; and due to soil evaporation in winter, soil is dry and deficit of moisture.
358 Observations show that with the progress of thawing, soil temperature and soil moisture
359 increase from top to bottom, and the thawing front deepens downward. Rainfall firstly
360 infiltrates to saturate the moisture deficit without runoff generation. Moreover, the existence
361 of the impermeable deeper frozen-soil layer leads to vertical disconnection between soil
362 water and groundwater. Although there is probably saturated water above the frozen soil
363 (Figure 3 and 7), the poor vertical connectivity largely hinders soil water percolation.
364 Without recharge to groundwater, there is limited runoff generation during the early
365 thawing.

366 At the end of the thawing season, as soon as the thaw depth reaches its maximum or
367 frozen-soil no longer exists, the frozen groundwater is released. The spikes in the observed
368 hydrograph are ~~is~~ likely due to different parts of the catchment reaching breakthrough,
369 which happens first in the lower elevations and then gradually moves upward to higher
370 landscape elements. This would trigger a sequence of sudden groundwater release and the
371 spikes. Snowfall is probably another influencing factor, causing the LRET and the spikes
372 phenomenon by storing precipitation as snow cover to reduce runoff, and releasing melting
373 water in a short time. This hypothesis needs to be tested by including snow accumulation
374 and melting processes in the hydrological model.

375 Once the soil is completely thawed at the end of the melting season, the rainfall-runoff
376 process returns to normal, and free of influence by the frozen-soil. Hence in the Hulu
377 catchment, frozen soil mainly impacts on streamflow during the freezing, frozen and
378 thawing periods.

379 Based on this perceptual model, we developed the conceptual framework of the frozen-soil
380 hydrological model, which needs to at least to consider the following elements: 1) we need
381 a semi-distributed modeling framework; 2) distributed forcing should be considered. 3)
382 different landscapes should be included; 4) topography should be involved, particularly
383 elevation; 5) we need to consider soil freeze/thaw processes; 6) snowfall and melting should
384 be included; 7) glacier melting should be included; 8) last but not least, the normal rainfall-
385 runoff processes are still important, because most runoff happen in the warm season, which
386 functions the same as in temperate climate regions.

4 A semi-distributed conceptual frozen-soil hydrology model

The perceptual model requires a quantitative conceptual model to test, revise, polish, verify, or even reject its hypotheses. Since the Hulu catchment has heterogenous landscapes, with a large elevation gradient, diverse land cover, and complex freeze/thaw process, we developed a semi-distributed frozen-soil hydrological model, i.e. FLEX-Topo-FS, based on the landscape-based hydrological modeling framework, i.e. FLEX-Topo. Numerous processes were involved in FLEX-Topo, including the distributed meteorological forcing, landscape heterogeneity, and snow and glacier melting. And in FLEX-Topo-FS, we explicitly considered the impacts of frozen-soil on soil water percolation and groundwater frozen processes in the supra-permafrost layer. The details of both the FLEX-Topo model (without frozen soil) and FLEX-Topo-FS model (with frozen soil) are described in below.

4.1 FLEX-Topo model (without frozen-soil)

4.1.1 Catchment discretization and meteorological forcing interpolation

The FLEX-Topo model classified the entire Hulu catchment into four landscapes, i.e. glaciers, alpine desert, vegetation hillslope, and riparian zone. The Hulu catchment (from 2960m to 4820m) was classified into 37 elevation bands, with 50m interval (Figure 2). Combined 4 landscapes and 37 elevation bands, we had 37×4=148 hydrological response units (HRUs). The structure of FLEX-Topo model consisted of four parallel components, representing the distinct hydrological function of different landscape elements (Savenije, 2010; Gao et al., 2014; Gharari et al., 2014; Gao et al., 2016). And the corresponding discharge of all elements was subsequently aggregated to obtain the simulated runoff.

We interpolated the precipitation (P) and temperature (T) based on elevation bands from in-situ observation (2980m) to each elevation band. The precipitation increasing rate was set as 4.2%/100m, and temperature lapse rate as -0.68°C/100m, based on field measurements (Han et al., 2013). Snowfall (P_s) or rainfall (P_l) was separated by air temperature, with the threshold temperature as 0°C (Gao et al., 2020).

4.1.2 Model description and configuration

FLEX-Topo is a semi-distributed conceptual bucket model (Savenije, 2010; Gao et al., 2014), with three modules, i.e. the snow and glacier module, the rainfall-runoff module, and the groundwater module. The water balance and constitutive equations can be found in Table 1. The model parameters and their prior ranges for calibration are listed in Table 2.

Snow and glacier module

The temperature-index method was employed to simulate snow and glacier melting (Gao et al., 2020). We used a snow reservoir (S_w) to account for the snow accumulating, melting (M_w) and water balance (Equation 4). The snow degree-day factor (F_{dd}) needs to be calibrated.

422   For glaciers, we assumed its area was constant in our simulation (from 2011 to 2014).

423   Glacier melting (M_g) was also calculated by the temperature-index method (Equation 7), but

424   with different degree-day factor. With the same air temperature, glacier has less albedo

425   than snow cover, thus with larger amount of melting. Glacier degree-factor was obtained by

426   multiplying snow degree-day factor (F_{dd}) with a correct factor C_g (Equation 8) (Gao et al.,

427   2020).

Rainfall-runoff module

429   There are two reservoirs to simulate rainfall-runoff process, including the root zone

430   reservoir (S_u) (Equation 10) and fast response reservoir (S_f) (Equation 17). To account of the

431   different rainfall-runoff processes in different landscapes and simultaneously avoid over

432   parameterization, we kept the same model structure for vegetation hillslope, riparian and

433   alpine desert (Equation 11, 12), but gave different root zone storage capacity (S_{umax}) values,

434   i.e. S_{umax_R} for riparian, S_{umax_D} for cold desert, and S_{umax_V} for hillslope vegetation. For vegetation

435   hillslope, a larger prior range was constrained for the root zone storage capacity (S_{umax_V}),

436   which means more water is required to fill in its storage capacity to meet its water deficit,

437   which is evidenced by previous studies in this region (Gao et al., 2014). For alpine desert,

438   due to its sparse vegetation cover, we constrained a shallower root zone storage capacity

439   (S_{umax_D}). For the riparian area, due to its location where is prone to be saturated, we also

440   constrained a shallower root zone storage capacity (S_{umax_R}). The initial states (beginning of

441   2011) of the reservoirs were obtained from the end values (end of 2014) of the simulation,

442   which is a normal procedure in modeling practice.

443   Other parameters in rainfall-runoff module (Equation 11-18, Table 1) include the threshold

444   value controlling evaporation (C_e), the shape parameter of the root zone reservoir (β), the

445   splitter (D) separating the generated runoff (R_u) from the root zone reservoir (S_u) to the fast

446   response reservoir, the recession parameter of faster reservoir (K_f), and the lag time from

447   rainfall event to peak flow (T_{lagF}). We set D as 0.2 from the isotope study (Ma et al., 2021).

448   And other parameters to be calibrated, with prior ranges (Table 2) based on previous

449   studies (Gao et al., 2014; Gao et al., 2020).

Groundwater module

451   The baseflow (Q_s) is generated from groundwater recession. The groundwater was

452   simulated by a linear reservoir (S_s) described in Section 3.2, and Equation 19. We set the

453   prior range for recession coefficient of baseflow reservoir (K_s) as (10-100 d). To estimate the

454   impacts of frozen groundwater on hydrological processes, we set the groundwater in

455   different landscapes as parallel. But we analyzed groundwater level as an integrated system,

456   because groundwater system is connected and this affects the groundwater level. Since the

457   sub-permafrost groundwater is even deeper than 20m in the Hulu catchment, and almost

458   disconnected to streamflow, thus we only model the supra-permafrost groundwater.

459    $$Q_s = S_s / K_s \quad (19)$$

460   ## 4.2 FLEX-Topo-FS model (with frozen soil)

461   ### 4.2.1 Modeling the soil freeze/thaw processes

462   FLEX-Topo-FS model employed the Stefan equation (Equation 20), to provide an
463   approximate solution to estimate freeze/thaw depth (Figure ~~10~~9). The Stefan equation is a
464   temperature-index based freeze-thaw algorithm, which assumes the sensible heat is
465   negligible in soil freeze/thaw simulation (Xie and Gough, 2013). The form of Stefan equation
466   is written as:

467    $$\varepsilon = \left(\frac{2 \cdot 86400 \cdot k \cdot F}{Q_L}\right)^{0.5} = \left(\frac{2 \cdot 86400 \cdot k \cdot F}{L \cdot \omega \cdot \rho}\right)^{0.5} \quad (20)$$

468   where ε is the freeze/thaw depth; k is the thermal conductivity (W/(m·K)) of the soil; F is the
469   surface freeze/thaw index. Freeze index (℃ degree-days) is the accumulated negative
470   ground temperature, while freezing; thaw index (℃ degree-days) is accumulated positive
471   ground temperature, while thawing. Q_L is the volumetric latent heat of soil, in J/m^3; and
472    $Q_L = L \cdot \omega \cdot \rho$ where L is the latent heat of fusion of ice (3.35·10^5 J/kg); ω is the water
473   content, as a decimal fraction of the dry soil weight; and ρ is the bulk density of the soil
474   (kg/m^3).

475   We set the thermal conductivity as k=2 W/(m·K), the water content as a decimal fraction of
476   the dry soil weight ω =0.12, and bulk density of the soil ρ=1000 kg/m^3 (Zhang et al.,
477   2019). Since the Stefan equation requires ground surface temperature, which is difficult to
478   measure and often lack of data, we used a multiplier to translate the air temperature to
479   ground temperature. The multiplier during freezing was set as 0.6, and during thawing we
480   assumed the ground surface temperature was the same as air temperature (Gisnås et al.,
481   2016).

482   In this model, we did not consider the impacts of snow cover on soil freeze/thaw, because
483   the snow effects were compiled in the Hulu catchment. Firstly, because precipitation in the
484   Hulu catchment mostly happens in summer as rainfall, and snow depth in the Hulu
485   catchment was less than 10mm in most area and time. Secondly, the snow cover has
486   contrary effects on ground temperature. Snow cover as an isolation layer increased ground
487   temperature in winter. But simultaneously snow cover also increased albedo, which
488   decreased net radiation, and decreased ground temperature. To avoid over
489   parameterization, we did not consider snow effect in the Stefan equation.

490   In this study, the Stefan equation was driven by distributed air temperature, which allowed
491   us to simulate the distributed soil freeze/thaw processes. With the distributed soil freeze
492   index and thaw index, we can also estimate the lower limit of permafrost, of which elevation
493   the freeze index equals to the thaw index in mountainous regions. Field survey on the lower
494   limit of permafrost (Wang et al., 2016) can provide another strong confirmation to our
495   simulated soil freeze/thaw process, except for the spot-scale freeze/thaw depth.

4.2.2 Modeling the impacts of frozen-soil on hydrology

The distributed freeze/thaw status calculated by FLEX-Topo-FS model allowed us to simulate the impacts of frozen-soil on soil and groundwater systems, their connectivity, and eventually catchment runoff.

In freezing and frozen seasons, precipitation was in the phase of snowfall, and topsoil was frozen, thus without surface runoff. During this period, runoff is only contributed from the groundwater discharge of the supra-permafrost layer (Q_s). There is no runoff generation (R_u) from the root zone reservoir to the response routine (S_s and S_f) in this period. In the conceptual model, we set $R_u = 0$ (Equation 11). In freezing season, when frozen depth was less than 3m (the depth of active layer in this region), the entire groundwater in the supra-permafrost layer were still connected~~functions~~, and could ~~was~~ be simulated by linear groundwater reservoir (S_s). Once the frozen depth of certain elevation zone is larger than 3m, the groundwater in that elevation zone was frozen (F_s). In the FLEX-Topo-FS model, we reduced the groundwater storage (S_s) to 10% of its total storage, to simulate its frozen status (Equation 21, 22). This amount of frozen water (F_s, 90% of groundwater storage when frozen, marked as $S_s(\tilde{t})$)) was~~does~~ held in the groundwater system as frozen-soil (Equation 22), but not disappeared~~, but held in the groundwater system as frozen-soil (Equation 22)~~. We set 90% frozen, rather than 100%, because there is still unfrozen liquid water in frozen-soil (Romanovsky and Osterkamp, 2000). Groundwater discharge was controlled by the frozen status, which was frozen from high elevations to lower elevations. This process is ~~like~~ progressively stopping the function of a series of cascade groundwater buckets, resulting in the discontinuous recession. Simultaneously, the decrease of discharge (Q_s) slowed down the decrease of groundwater level (S_s). This conceptual model allowed us to simulate the bend down of baseflow recession and slower decreasing of groundwater level.

$$\frac{\mathrm{d}S_s}{\mathrm{d}t} = R_s - Q_s - F_s \quad (21)$$

$$F_s = \begin{cases} 0.9 \cdot S_s(\tilde{t}); & \text{once } freeze\ depth \geq 3m \\ -0.9 \cdot S_s(\tilde{t}); & \text{once } thaw\ depth \text{ reach to yearly max} \\ & \text{or } thaw\ depth \geq freeze\ depth \end{cases} \quad (22)$$

In ~~early~~ thawing seasons, the freeze/thaw condition in the lowest elevation zone plays a key role, controlling the hydraulic connectivity between soil and groundwater systems. In the conceptual model, if freeze depth calculated by Stefan equation is larger than thaw depth, this means the frozen layer still exists, which obstructs the soil and groundwater connection. In the conceptual model, we kept as the runoff generation $R_u = 0$ (Equation 11). Since there is no percolation from soil to groundwater, and root zone soil moisture (S_u) is accumulating, even ponding in some local depressions (Figure 7). The only outflow of the root zone is evaporation in this period. This conceptual model allowed us to reproduce the LRET observation. For groundwater reservoir, once the thaw depth goes to its yearly maximum (in permafrost area) or thaw depth > freeze depth (in seasonal frozen-soil area), the frozen

532 water (90% of groundwater storage when frozen, $S_s(\tilde{t})$) was released to the groundwater

533 again (Equation 22). The sudden release of frozen groundwater causes the spikes in
534 hydrograph, which could happen in either thawing seasons or complete thaw seasons
535 depending on its elevation. But in either way, the water balance calculation is one-hundred-
536 percent closed.

537 Complete thaw in the lowest elevation marked the end of thawing season, and the start of
538 complete thaw season. In the complete thaw season, soil water and groundwater are
539 connected, and runoff generation (R_u) returns to normal circumstances, which can be
540 simulated by the FLEX-Topo model without frozen-soil.

4.3 Model uncertainty analysis and evaluation metrics

542 The Kling-Gupta efficiency (Gupta et al., 2009; KGE) was used as the performance metric in
543 model calibration:

$$KGE = 1 - \sqrt{(r-1)^2 + (\alpha - 1)^2 + (\beta - 1)^2} \qquad (23)$$

545 Where r is the linear correlation coefficient between simulation and observation; α ($\alpha =$
546 σ_m/σ_o) is a measure of relative variability in the simulated and observed values, where σ_m is
547 the standard deviation of simulated variables, and σ_o is the standard deviation of observed
548 variables; β is the ratio between the average value of simulated and observed variables.

549 We applied the Generalized Likelihood Uncertainty Estimation framework (GLUE, Beven and
550 Binley, 1992) to estimate model parameter uncertainty. Sampling the parameter space with
551 20, 000 parameter sets, and select the top 1% parameter as behavioral parameter sets.

552 For a comprehensive assessment of model performance in validation, the behavioral model
553 runs were evaluated using multiple criteria, including KGE, KGL (the KGE of logarithms flow,
554 and more sensitive to baseflow), Nash-Sutcliffe Efficiency (NSE) (Nash and Sutcliffe, 1970)
555 (Equation 24), coefficient of determination (R^2) and root mean square error (RMSE).

$$NSE = 1 - \frac{\sum_{t=1}^{n}(Q_o - Q_m)^2}{\sum_{t=1}^{n}(Q_o - \overline{Q_o})^2} \quad (24)$$

557 Where Q_o is observed runoff, $\overline{Q_o}$ is the observed average runoff, and Q_m is modeled runoff.

558 The model was calibrated in the period 2011-2012, and uses KGE as objective function. The
559 second half time series (2013-2014) were used to quantify the model performance in
560 streamflow split-sample validation, with multi-criteria including KGE, KGL, NSE, R^2, and
561 RMSE. The KGE, KGL, NSE and R^2 are all less than 1, and their valuation closer to 1 indicates
562 better model performance. While the less value of RMSE indicates less error and better
563 performance.

5 Testing the realism of FLEX-Topo-FS model

5.1 FLEX-Topo model results and its discrepancy

Figure 109 shows that the FLEX-Topo model can somehow reproduce the observed hydrography in most periods, except for the LRET and DBR events. In calibration, the KGE was 0.78. And in validation, the KGE =0.58, KGL =0.36, NSE =0.41, R^2= 0.82, and RMSE = 0.95mm/d. While taking account the impacts of landscape heterogeneity, the FLEX-Topo model can to some extent simulate the LRET phenomenon. The vegetated hillslope in relatively lower elevation has larger unsaturated storage capacity, with larger soil moisture deficit in the beginning of melting season, and capable to hold more rainfall with initial dry soil. Moreover, FLEX-Topo model has took snow accumulation and melting into account, which also reduced the runoff generation during the LRET periods. However, there was still large overestimation in the early thawing season.

Additionally, the simulated hydrography on logarithm scale clearly shows that the baseflow is the result of a linear reservoir (Figure 109). The linear reservoir model can mimic recession quite well in the beginning of baseflow recession, but the model discrepancy becomes larger in the middle to the end of frozen season. Hence, FLEX-Topo model is not able to simulate the discontinuous recession. The model discrepancy indicates that without considering frozen-soil, FLEX-Topo cannot well reproduce the observed LRET and DBR observations, although explicitly considered landscape heterogeneity, snow and glacier processes.

5.2 FLEX-Topo-FS model results

5.2.1 Freeze/thaw simulation by FLEX-Topo-FS model

Figure 10 9 demonstrates that the Stefan equation was capable to reproduce the freeze/thaw process. This verified the success of the freeze/thaw parameterization and the parameter sets. Also, the simulated lower limit of permafrost is 3716m, which is largely close to field survey in the upper Heihe River basin, around 3650 – 3700 m (Wang et al., 2016), and the expert-based estimation of 3650 m of Hulu catchment. Both the well reproduced freeze/thaw variation in spot scale, and the lower limit of permafrost in catchment scale, gave us strong confidence to the simulation of soil freeze/thaw processes.

5.2.2 Runoff simulation by FLEX-Topo-FS model

While considering the impacts of frozen-soil, the FLEX-Topo-FS model, compared with FLEX-Topo, dramatically improved the model performance. Figure 11 10 showed the simulated hydrograph by FLEX-Topo-FS on both normal and log scales. Both the LRET and the DBR observations were almost perfectly reproduced by the FLEX-Topo-FS model. The

KGE of FLEX-Topo-FS in calibration was 0.78, which was the same as FLEX-Topo. But in validation, the performance was significantly improved, the KGE improved from 0.58 to 0.66, KGL was from 0.36 to 0.72, NSE was from 0.41 to 0.60, R^2 from 0.82 to 0.83, and RMSE was reduced from 0.95mm/d to 0.79mm/d. All the model evaluation criteria were improved. The most significant improvement was the baseflow simulation, and KGL was increased from 0.36 to 0.72. We also noted that the FLEX-Topo-FS model reproduced the spikes during the thawing in Figure 10~~1~~. This further confirms our conceptual model of a sequence of thawing breakthroughs, which trigger the sudden release of groundwater starting at lower elevations and progressing to higher landscape elements.

5.2.3 Modeling groundwater trends

To further verify the FLEX-Topo-FS model, we averaged the simulated groundwater storage (S_s) of all HRUs, and compared with the observed groundwater depth on log scale (Figure 11~~2~~). We included the frozen groundwater in the total groundwater storage (S_s), because the liquid groundwater is in connection with the frozen groundwater and this affects the groundwater level variation. Figure 11~~2~~ clearly demonstrated that the simulated groundwater storage decreased slower, and the time scale of recession was increased. The trends of simulated groundwater storage and observed groundwater level, which are not the same, but similar physical meaning describing groundwater dynamic, correspond surprisingly well. This is particularly encouraging, given that the periods of simulation (2011-2014) and observation (2016-2019) were not overlaid, and a point observation may not be straightforwardly representative for the entire basin.

The success to reproduce groundwater level trends is another strong confirmation for the FLEX-Topo-FS model. All the successes of FLEX-Topo-FS model to reproduce spot scale freeze/thaw depth variation, lower limit of permafrost, LRET and DBR events, and groundwater level trends, gave us strong confidence to the realism of our qualitative perceptual model and quantitative conceptual model.

6 Discussion

6.1 Diagnosing the impacts of frozen-soil on complex mountainous hydrology

6.1.1 Understanding complex frozen-soil hydrology by hydrography analysis

Frozen-soil happens underneath, with frustrating spatial-temporal heterogeneities, and difficulty to measure. Although there are spot and hillslope measurements, its impact on catchment hydrology is still hard to explore. Hydrography, easily and widely observed and globally accessible, can be regarded as the by-product of the entire catchment hydrological system (Gao, 2015). Hydrography as an integrated signal provides us a vital source of information, reflecting how the complex hydrological system works, i.e. transforming

634 precipitation into runoff. Hence, hydrography itself is a valuable source of data to
635 understand catchment frozen-soil hydrology.

636 Especially the baseflow embodies the influence of basin characteristics including the
637 geology, soils, morphology, vegetation, and frozen-soil (Blume et al., 2007; Ye et al., 2009).
638 Hence, the quantitative description of baseflow is a valuable tool for understanding how the
639 groundwater system behaves (McNamara et al., 1998). Baseflow recession was used to
640 identify the impacts of climate change on permafrost hydrology. In previous studies,
641 Slaughter and Kane (1976) found that basins with permafrost have higher peak flows and
642 lower baseflows. The baseflow, representing groundwater recession, provides important
643 information about the storage capacity and recession characteristics of the active layer in
644 permafrost regions (Brutsaert, and Hiyama, 2012).

645 Moreover, hydrological system has tremendous influencing factors. The hydrograph of
646 paired catchments provides a good reference, as a controlled experiment, to isolate one
647 influencing factor from the others. Nested catchments helped us to acknowledge the
648 importance of region-specific knowledge, which is often the key to interpret the
649 unexplained variability of large sample studies (Fenicia and McDonnell, 2022). In this study,
650 the pair catchment method helped us to confirm the impacts of frozen-soil on LRET and
651 DBR observations.

652 ~~Moreover~~Additionally, by analyzing the nested sub-basins of the Lena River in Siberia, Ye et
653 al. (2008) used the peak flow/baseflow ratio to quantify the impact of permafrost coverage
654 on hydrograph regime in Lena River basin, and found that frozen-soil only affects discharge
655 regime over high permafrost regions (greater than 60%), and no significant affect over the
656 low permafrost (less than 40%) regions. In this study, we reconfirmed this statement. The
657 permafrost area proportions of the Hulu catchment and Zhamashike sub-basin are 64% and
658 74%, with significant effects on discharge, while 38% of the Qilian sub-basin is covered by
659 permafrost, with no significant effects on discharge regime.

660 By paired catchments comparison, interestingly, the K_s in Zhamashike and Qilian in the early
661 recession period are both 60d, which is exactly within the standard value of 45±15 days
662 derived in earlier studies for basins ranging in size between 1,000 and 100,000 km^2
663 (Brutsaert and Sugita, 2008; Brutsaert and Hiyama, 2012), which was likely the results of
664 catchment self-similarity and co-evolution. But we also noticed that the K_s in the small Hulu
665 catchment (K_s = 80d and 60d) is quite larger than the Zhamashike (K_s = 60d and 20d) and
666 Qilian (K_s = 60d). This could be rooted in different scale and drainage density (Brutsaert and
667 Hiyama, 2012). The Hulu catchment is located in the headwater with less drainage density,
668 hence less contact area between hillslope and river channel, slower baseflow recession, and
669 larger K_s value. We argue that even without the impacts from frozen-soil, it is difficult to
670 give accurate K_s estimation in small catchments (less than 1,000 km^2) in moderate climates. It
671 is more substantial difficult to estimate the discontinuous K_s in different periods in frozen-
672 soil catchments without calibration. Thus, estimating the value of recession coefficient (K_s) in
673 different catchments and periods, especially for small catchments and in cold regions, is still
674 an intriguing scientific question for hydrologists.

675 ~~the validity of the standard value of K_s (45±15 days), in small catchments less than 1,000~~

676 ~~km², may need more studies.~~

6.1.2 Understanding complex frozen-soil hydrology by multi-source observations

678 Observation is still a bottleneck in complex mountainous cold regions. Traditionally,
679 fragmented observations are only for specific variables, like puzzles. In this study, we
680 collected multi-source data, including soil moisture, groundwater level, topography,
681 geology survey, isotope, soil temperature, freeze/thaw depth, permafrost and seasonal
682 frozen-soil map, and hydrograph in paired catchments. Multi-source data analysis provides
683 multi-dimensional perspective to investigate frozen-soil hydrology. We argue that on one
684 hand, multi-source observations helped us to deliver the perceptual and conceptual
685 models. And on the other hand, perceptual and conceptual models bridge the gap between
686 experimentalists and modelers (Seibert and McDonnell, 2002), allowing us put fragmented
687 observations together, and understand the hydrological system in an integrated and
688 qualitative way.

689 Data gap is a common issue in mountainous hydrology studies. For example, in this study,
690 runoff data has a gap period in the end of thawing season in 2013, due to flooding and
691 equipment malfunction. Soil moisture and groundwater level data had large gap, which
692 cannot be used for continuous modeling. Luckily, the meteorological data, which is
693 important forcing data to run the models, was continuous without any gap. With sufficient
694 meteorological forcing data, we successfully run the hydrological models from 2011 to
695 2014. The runoff data gap in the end of thawing season in 2013 merely influenced model
696 validation. While evaluating models, we did not involve the data gap period. Hence, the
697 data gap does not have any impact on the consolidation of the conclusions.

698 Although soil moisture had large gap, fortunately there were some observations during the
699 LRET periods, which were sufficient to distinguish the impacts of frozen soil on soil moisture
700 profile. Additionally, although the groundwater level observation (2016-2019) was not
701 overlaid with other hydrometeorological measurements (2011-2014), its repeating seasonal
702 pattern allowed us to qualitatively understand how groundwater system behaves.
703 Groundwater fluctuation in natural catchments has strong periodicity, which can be
704 observed in Figure 11. Groundwater variation does not show significant difference among
705 different years, which is especially true for the 25m well. Due to the extreme difficulty of
706 continuous observation in this region, there was no groundwater measurement in 2011-
707 2014. But due to the strong repeated temporal variation of groundwater level, we have
708 good reason to believe the trends in 2016-2019 also happened in 2011-2014. Moreover,
709 this is a qualitative comparison, rather than a quantitative one, which we do not think has
710 any impact on our conclusions.~~Hence, the data gap does not have any impact on the~~
711 ~~consolidation of the conclusions.~~

712 In general, we argue that data gap always exists. In another words, we can never have
713 sufficient data. The only thing we can do is using the accessible data to understand
714 processes. ~~In this study, although soil moisture had large gap, fortunately there were some~~
715 ~~observations during the LRET periods, which were sufficient to distinguish the impacts of~~
716 ~~frozen soil on soil moisture profile. Additionally, although the groundwater level observation~~

717 ~~(2016–2019) was not overlaid with other hydrometeorological measurements (2011–2014),~~
718 ~~its repeating seasonal pattern allowed us to qualitatively understand how groundwater~~
719 ~~system behaves.~~ Although~~We argue that~~ perfect data does not exist, ~~but~~ with more multi-
720 source and better data quality, the more accurate understanding we can achieve. This needs
721 the close collaboration among multi-disciplinary researchers, including but not limited to
722 hydrologists, meteorologists, ecologists, geocryologists, geologists, and engineers.

723 **6.1.3 Understanding complex frozen-soil hydrology by model discrepancy**

724 By a simple water balance inspection, we found that the total annual runoff of Hulu
725 catchment was 499mm/a, which is even larger than the observed annual precipitation
726 433mm/a. This means that without considering distributed meteorological forcing, the
727 runoff coefficient is larger than 1, and the water balance cannot be closed. This result is also
728 in line with previous studies, showing that precipitation in mountainous areas is largely
729 underestimated (Immerzeel et al., 2015; Chen et al., 2018; Zhang et al., 2018b).

730 Although the semi-distributed FLEX-Topo has considered tremendous processes, including
731 rainfall-runoff processes, distributed forcing, landscape heterogeneity, topography, snow
732 and glacier melting, there was still model discrepancy to reproduce the LRET and DBR
733 observations. This means there must be some processes missed in the model. After our
734 expert-driven data analysis, we attributed the model discrepancy to soil freeze/thaw
735 processes.

736 Model fitness is the goal which all modelers are pursuing. But we argue that in many cases,
737 model discrepancy can tell us more interesting things than perfect fitting. In this study, we
738 used the FLEX-Topo model, without frozen-soil, as a diagnosing tool to understand the
739 possible impacts of frozen-soil on the complex mountainous hydrology. Using tailor-made
740 hydrological model and integrated observations as diagnostic tools is a promising approach
741 to step-wisely understand the complex mountainous hydrology.

742 **6.2 Modeling frozen-soil hydrology: top-down VS bottom-up**

743 Top-down and bottom-up are two philosophies for model development (Sivalpalan et al.,
744 2003). The bottom-up approach attempts to model catchment scale response based on the
745 prior knowledge learned in small scale. Bottom-up approach is commonly used in frozen-
746 soil hydrological modeling, because this is straightforward. And for modeling, it is a
747 common practice to experiment with/without a certain process, and claim its impacts on
748 runoff. But the bottom-up modeling largely missed the key step to diagnose the impacts of
749 small-scale processes on catchment response. Lack of process understanding usually leads
750 modeling studies to data pre- and pro-processing and extensive parameter calibration with
751 the risk of equifinality and model malfunction.

752 By our expert-driven top-down modeling approach, we firstly tried to understand the
753 hydrological processes at work, using multi-source data and analysing model discrepancy.
754 We then translated our understanding to perceptual and conceptual models. The top-down

755 method is an appealing way to identify the key influencing factors, rather than being lost in
756 endless details and heterogeneities. Such informed analysis of the data helps to bring
757 experimentalist insights into the initiation of the conceptual model construction.

758 ## 6.3 ~~Climate change~~Warming impacts on frozen-soil hydrology

759 To quantify the impacts of ~~climate change~~warming on frozen-soil hydrology, we arbitrarily
760 set the air temperature increased by 2°C. The FLEX-Topo-FS simulation illustrated that
761 complete thaw date became 16-19 days earlier, and the lower limit of permafrost increased
762 by 294 m, from 3716m to 4010m. For runoff simulation, the DBR phenomenon became less
763 obvious (Figure ~~13~~12). This is because two-degree warming results in permafrost
764 degradation, which means most permafrost is degraded to seasonal frozen-soil. Since the
765 DBR was caused by the different groundwater discharge behaviors in permafrost and
766 seasonal frozen-soil areas. Specially, the first recession period was contributed by the
767 groundwater discharge from both permafrost and seasonal frozen-soil areas, and the
768 second recession period was only from the seasonal frozen-soil area. The permafrost
769 degradation turns most permafrost into seasonal frozen-soil, and makes groundwater
770 discharge nearly only from the seasonal frozen-soil region, and leads to more continuous
771 baseflow recession. Eventually, warming leads to the increase of b~~B~~oth the baseflow and
772 runoff in early thawing seasons ~~were increased~~. Th~~is means climate change will increase~~e
773 warming effect on baseflow~~, which phenomenon~~ was already widely observed in Arctic and
774 mountainous permafrost rivers (Ye et al., 2009; Brutsaert et al., 2012; Niu et al., 2010; Song
775 et al., 2020). Hence, th~~is result~~ese wide observations could be another verification for the
776 FLEX-Topo-FS model realism. For implications in water resource management, the results
777 indicate that frozen soil degradation caused by climate change may largely alter streamflow
778 regime, especially for the thirsty spring and early summer, in vast cold ~~Tibetan Plateau~~QTP.
779 It is also worthwhile to be noted that this is ~~very~~ primary prediction. We used 2 degrees
780 warmer more like using a sensitive analysis to illustrate how warming will impact on
781 baseflow, to further verify the capability and robustness of the model itself. ~~And~~In future
782 studies, we need more detailed ~~studies~~modelling studies to use the state-of-the-art
783 climate prediction and downscaling methodologies, to assess the frozen-soil change and
784 hydrology variations ~~in future~~.

785 ## 6.4 Implications for other cold regions

786 We believe that the FLEX-Topo-FS model has great potential to be applied in other cold
787 regions. There are mainly three reasons.

788 Firstly, our study site, the Hulu catchment, although small (23.1 km^2), has a large elevation
789 gradient (from 2960 m to 4820 m), diverse landscapes (hillslope vegetation, riparian area,
790 alpine desert, and glaciers), snowfall and snowmelt, and both permafrost and seasonal
791 frozen-soil. Our newly developed model explicitly considered all these spatial and temporal
792 heterogeneities, and eventually achieved excellent performance. With such a comprehensive
793 modeling toolkit, the model has potential to be upscaled or transfer to other cold regions.

794 Secondly, we obtained the perceptual model from not only the observations and our expert
795 knowledge at the Hulu catchment itself, but also widely considered the impact of frozen-
796 soil on hydrological processes in other catchments, including the Zhamashike and Qilian
797 (two nested sub-catchments of the upper Heihe), the headwater of Yellow River, and the
798 Cape Bounty Arctic Watershed Observatory in Canada. Thus, we developed the model for
799 the Hulu catchment in the context of larger scale observations.

800 Thirdly, the realism of the conceptual model was confirmed not only by streamflow
801 measurement, but also by multi-source and multi-scale observations, particularly the
802 freezing and thawing front in the soil, the lower limit of permafrost, and the trends in
803 groundwater level variation.

804 Although our new model generally has great potential to be used in other cold regions, we
805 should be cautious to arbitrarily use the model without any prior understanding of the
806 modeling system. Since frozen-soil is merely one influential factor for cold region
807 hydrology, there are other factors having notable impacts, which are intertwined with
808 frozen-soil. This relates especially to the geology condition, which can have considerable
809 impact on frozen-soil, but has large spatial heterogeneity, and where it is difficult to take
810 measurements. For the model empirical parameters, most of them are related to the freeze-
811 thaw processes related to Stefan equation, which have clear physical meanings, and
812 confirmed by previous studies with a good spatial distribution over the entire QTP (e.g. Zou
813 et al., 2017; Ran et al., 2022). Due to the extreme complexity of soil and geology in
814 mountainous catchment, we still need to recalibrate their values while modeling other
815 basins on the QTP. Hence, before upscaling to other cold regions, we recommend to follow
816 a stringent modeling procedure, i.e expert-driven data analysis → qualitative perceptual
817 model → quantitative conceptual model → testing of model realism.

7 Conclusions

819 Our knowledge on frozen-soil hydrology is still incomplete, which is particularly true for
820 complex mountainous catchment on the ~~Tibetan Plateau~~QTP. In the past decades, we have
821 collected numerous heterogeneities and complexities in frozen-soil regions, but most of
822 these observations are still neither well integrated into hydrological models, nor used to
823 constrain model structure or parameterization in catchment-scale studies. More
824 importantly, we still largely lack quantitative knowledge on which variables play more
825 dominant roles at certain spatial-temporal scales, and should be included in models with
826 priority.

827 By conducting this frozen-soil hydrological modeling study for the complex mountainous
828 Hulu catchment, we reached the following conclusions: 1) we observed two new
829 phenomena in the frozen-soil catchment, i.e. the low runoff in early thawing seasons (LRET)
830 and discontinuous baseflow recession (DBR), which are widespread but not yet reported; 2)
831 without considering the frozen-soil, the FLEX-Topo model was not able to reproduce LRET
832 and DBR observations; 3) considering frozen-soil impacts on soil-groundwater connectivity,
833 and groundwater recession, the FLEX-Topo-FS model successfully reproduced the LRET and

834 DBR events. The FLEX-Topo-FS results were also verified by observed freeze/thaw depth
835 variation, groundwater level, and lower limit of permafrost. We believe this study is able to
836 give us new insights into further implications to understand the impact of frozen soil on
837 hydrology, projecting the impacts of climate change on water resources in vast cold regions,
838 which is one of the 23 major unsolved scientific problems in hydrology community.

839

840 **ACKNOWLEDGMENTS**

841 This study was supported by the National Natural Science Foundation of China (Grant Nos.
842 42122002, 42071081, 42171125, and 41971041).

843

References:

845 Andresen, C. G., Lawrence, D. M., Wilson, C. J., David McGuire, A., Koven, C., Schaefer, K.,
846 Jafarov, E., Peng, S., Chen, X., Gouttevin, I., Burke, E., Chadburn, S., Ji, D., Chen, G., Hayes, D.
847 and Zhang, W.: Soil moisture and hydrology projections of the permafrost region-a model
848 intercomparison, Cryosphere, 14(2), 445–459, doi:10.5194/tc-14-445-2020, 2020.

849 Beven, K. and Binley, A.: The future of distributed models: Model calibration and uncertainty
850 prediction, Hydrol. Process., 6(3), 279–298, doi:10.1002/hyp.3360060305, 1992.

851 Blume, T., Zehe, E. and Bronstert, A.: Rainfall-runoff response, event-based runoff
852 coefficients and hydrograph separation, Hydrol. Sci. J., 52(5), 843–862,
853 doi:10.1623/hysj.52.5.843, 2007.

854 Blöschl, G., Bierkens, M. F. P., Chambel, A., et al.: Twenty-three unsolved problems in
855 hydrology (UPH)–a community perspective, Hydrol. Sci. J., 64(10), 1141–1158,
856 doi:10.1080/02626667.2019.1620507, 2019.

857 Bring, A., Fedorova, I., Dibike, Y., Hinzman, L., Mård, J., Mernild, S. H., Prowse, T., Semenova,
858 O., Stuefer, S. L. and Woo, M. K.: Arctic terrestrial hydrology: A synthesis of processes,
859 regional effects, and research challenges, J. Geophys. Res. G Biogeosciences, 121(3), 621–
860 649, doi:10.1002/2015JG003131, 2016.

861 Brutsaert, W. and Sugita, M.: Is Mongolia's groundwater increasing or decreasing? The case
862 of the Kherlen River basin, Hydrol. Sci. J., 53(6), 1221–1229, doi:10.1623/hysj.53.6.1221,
863 2008.

864 Brutsaert, W. and Hiyama, T.: The determination of permafrost thawing trends from long-
865 term streamflow measurements with an application in eastern Siberia, J. Geophys. Res.
866 Atmos., 117(22), 1–10, doi:10.1029/2012JD018344, 2012.

867 Bui, M. T., Lu, J. and Nie, L.: A review of hydrological models applied in the permafrost-
868 dominated Arctic region, Geosci., 10(10), 1–27, doi:10.3390/geosciences10100401, 2020.

869 Cao, B., Zhang, T., Wu, Q., Sheng, Y., Zhao, L. and Zou, D.: Permafrost zonation index map

870 and statistics over the Qinghai–Tibet Plateau based on field evidence, Permafr. Periglac.
871 Process., 30(3), 178–194, doi:10.1002/ppp.2006, 2019.

872 Chadburn, S., Burke, E., Essery, R., Boike, J., Langer, M., Heikenfeld, M., Cox, P. and
873 Friedlingstein, P.: An improved representation of physical permafrost dynamics in the JULES
874 land-surface model, Geosci. Model Dev., 8(5), 1493–1508, doi:10.5194/gmd-8-1493-2015,
875 2015.

876 Chang, J., Wang, G. X., Li, C. J. and Mao, T. X.: Seasonal dynamics of suprapermafrost
877 groundwater and its response to the freeing-thawing processes of soil in the permafrost
878 region of Qinghai-Tibet Plateau, Sci. China Earth Sci., 58(5), 727–738, doi:10.1007/s11430-
879 014-5009-y, 2015.

880 Chen, R., Song, Y., Kang, E., Han, C., Liu, J., Yang, Y., Qing, W. and Liu, Z.: A cryosphere-
881 hydrology observation system in a small alpine watershed in the Qilian mountains of China
882 and its meteorological gradient, Arctic, Antarct. Alp. Res., 46(2), 505–523, doi:10.1657/1938-
883 4246-46.2.505, 2014.

884 Chen, R., Wang, G., Yang, Y., Liu, J., Han, C., Song, Y., Liu, Z. and Kang, E.: Effects of
885 Cryospheric Change on Alpine Hydrology: Combining a Model With Observations in the
886 Upper Reaches of the Hei River, China, J. Geophys. Res. Atmos., 123(7), 3414–3442,
887 doi:10.1002/2017JD027876, 2018.

888 Chiasson-Poirier, G., Franssen, J., Lafrenière, M. J., Fortier, D. and Lamoureux, S. F.: Seasona
889 evolution of active layer thaw depth and hillslope-stream connectivity in a permafrost
890 watershed, Water Resour. Res., 56(1), 1–18, doi:10.1029/2019WR025828, 2020.

891 Cuo, L., Zhang, Y., Bohn, T. J., Zhao, L., Li, J., Liu, Q. and Zhou, B.: Journal of geophysical
892 research, Nature, 175(4449), 238, doi:10.1038/175238c0, 1955.

893 Ding, Y., Zhang, S., Chen, R., Han, T., Han, H., Wu, J., Li, X., Zhao, Q., Shangguan, D., Yang, Y.,
894 Liu, J., Wang, S., Qin, J. and Chang, Y.: Hydrological Basis and Discipline System of
895 Cryohydrology: From a Perspective of Cryospheric Science, Front. Earth Sci., 8(December),
896 doi:10.3389/feart.2020.574707, 2020.

897 Dobinski, W.: Permafrost. Earth-Science Reviews, 108, 158–169, 2011.

898 Evans, S. G., Ge, S., Voss, C. I. and Molotch, N. P.: The Role of Frozen Soil in Groundwater
899 Discharge Predictions for Warming Alpine Watersheds, Water Resour. Res., 54(3), 1599–
900 1615, doi:10.1002/2017WR022098, 2018.

901 Fabre, C., Sauvage, S., Tananaev, N., Srinivasan, R., Teisserenc, R. and Pérez, J. M. S.: Using
902 modeling tools to better understand permafrost hydrology, Water (Switzerland), 9(6),
903 doi:10.3390/w9060418, 2017.

904 Farquharson, L. M., Romanovsky, V. E., Cable, W. L., Walker, D. A., Kokelj, S. V. and Nicolsky,
905 D.: Climate Change Drives Widespread and Rapid Thermokarst Development in Very Cold
906 Permafrost in the Canadian High Arctic, Geophys. Res. Lett., 46(12), 6681–6689,
907 doi:10.1029/2019GL082187, 2019.

908 Fenicia, F., Savenije, H. H. G., Matgen, P. and Pfister, L.: Is the groundwater reservoir linear?
909 Learning from data in hydrological modelling, Hydrol. Earth Syst. Sci., 10(1), 139–150,
910 doi:10.5194/hess-10-139-2006, 2006.

911 Fenicia, F., Kavetski, D. and Savenije, H. H. G.: Elements of a flexible approach for conceptual
912 hydrological modeling: 1. Motivation and theoretical development, Water Resour. Res.,
913 47(11), 1–13, doi:10.1029/2010WR010174, 2011.

914 Fenicia, F. and McDonnell, J. J.: Modeling streamflow variability at the regional scale: (1)
915 perceptual model development through signature analysis, J. Hydrol., 605(December 2021),
916 127287, doi:10.1016/j.jhydrol.2021.127287, 2022.

917 Gao, B., Yang, D., Qin, Y., Wang, Y., Li, H., Zhang, Y. and Zhang, T.: Change in frozen soils
918 and its effect on regional hydrology, upper Heihe basin, northeastern Qinghai-Tibetan
919 Plateau, Cryosphere, 12(2), 657–673, doi:10.5194/tc-12-657-2018, 2018.

920 Gao, H., Hrachowitz, M., Fenicia, F., Gharari, S. and Savenije, H. H. G.: Testing the realism of a
921 topography-driven model (FLEX-Topo) in the nested catchments of the Upper Heihe, China,
922 Hydrol. Earth Syst. Sci., 18(5), 1895–1915, doi:10.5194/hess-18-1895-2014, 2014.

923 Gao, H.: Landscape-based hydrological modelling: understanding the influence of climate,
924 topography, and vegetation on catchment hydrology, Ph.D. Dissertation, Delft University of
925 Technology, 2015

926 Gao, H., Hrachowitz, M., Sriwongsitanon, N., Fenicia, F., Gharar, S.i, and Savenije, H. H. G.:
927 Water Resources Research, J. Am. Water Resour. Assoc., 5(3), 2–2, doi:10.1111/j.1752-
928 1688.1969.tb04897.x, 1969.

929 Gao, H., Ding, Y., Zhao, Q., Hrachowitz, M. and Savenije, H. H. G.: The importance of aspect
930 for modelling the hydrological response in a glacier catchment in Central Asia, Hydrol.
931 Process., 31(16), 2842–2859, doi:10.1002/hyp.11224, 2017.

932 Gao, H., Dong, J., Chen, X., Cai, H., Liu, Z., Jin, Z., Mao, D., Yang, Z. and Duan, Z.: Stepwise
933 modeling and the importance of internal variables validation to test model realism in a data
934 scarce glacier basin, J. Hydrol., 591(September), 125457, doi:10.1016/j.jhydrol.2020.125457,
935 2020.

936 Gao, H., Wang, J., Yang, Y., Pan, X., Ding, Y. and Duan, Z.: Permafrost Hydrology of the
937 Qinghai-Tibet Plateau: A Review of Processes and Modeling, Front. Earth Sci., 8(January),
938 doi:10.3389/feart.2020.576838, 2021.

939 Gao, J., Xie, Z., Wang, A., Liu, S., Zeng, Y., Liu, B., Li, R., Jia, B., Qin, P. and Xie, J.: A New
940 Frozen Soil Parameterization Including Frost and Thaw Fronts in the Community Land
941 Model, J. Adv. Model. Earth Syst., 11(3), 659–679, doi:10.1029/2018MS001399, 2019.

942 Gharari, S., Hrachowitz, M., Fenicia, F., Gao, H. and Savenije, H. H. G.: Using expert
943 knowledge to increase realism in environmental system models can dramatically reduce the
944 need for calibration, Hydrol. Earth Syst. Sci., 18(12), 4839–4859, doi:10.5194/hess-18-4839-
945 2014, 2014.

946 Gisnas, K., Westermann, S., Vikhamar Schuler, T., Melvold, K. and Etzelmüller, B.: Small-scale
947 variation of snow in a regional permafrost model, Cryosphere, 10(3), 1201–1215,
948 doi:10.5194/tc-10-1201-2016, 2016.

949 Gouttevin, I., Krinner, G., Ciais, P., Polcher, J. and Legout, C.: Multi-scale validation of a new
950 soil freezing scheme for a land-surface model with physically-based hydrology, Cryosphere,
951 6(2), 407–430, doi:10.5194/tc-6-407-2012, 2012.

952 Gupta, H. V., Kling, H., Yilmaz, K. K. and Martinez, G. F.: Decomposition of the mean squared
953 error and NSE performance criteria: Implications for improving hydrological modelling, J.
954 Hydrol., 377(1–2), 80–91, doi:10.1016/j.jhydrol.2009.08.003, 2009.

955 Han, C., Chen, R., Liu, J., Yang, Y., Liu, Z.: Hydrological characteristics in non-freezing period
956 at the alpine desert zone of Hulugou watershed, Qilian Mountains. Journal of Glaciology
957 and Geocryology, 35(6), 1536-1544, 2013.

958 Han, C., Chen, R., Liu, Z., Yang, Y., Liu, J., Song, Y., Wang, L., Liu, G., Guo, S. and Wang, X.:
959 Cryospheric Hydrometeorology Observation in the Hulu Catchment (CHOICE), Qilian
960 Mountains, China, Vadose Zo. J., 17(1), 180058, doi:10.2136/vzj2018.03.0058, 2018.

961 Hülsmann, L., Geyer, T., Schweitzer, C., Priess, J. and Karthe, D.: The effect of subarctic
962 conditions on water resources: initial results and limitations of the SWAT model applied to
963 the Kharaa River Basin in Northern Mongolia, Environ. Earth Sci., 73(2), 581–592,
964 doi:10.1007/s12665-014-3173-1, 2015.

965 Immerzeel, W. W., Van Beek, L. P. H. and Bierkens, M. F. P.: Climate change will affect the
966 asian water towers, Science (80-.)., 328(5984), 1382–1385, doi:10.1126/science.1183188,
967 2010.

968 Immerzeel, W. W., Wanders, N., Lutz, A. F., Shea, J. M. and Bierkens, M. F. P.: Reconciling
969 high-altitude precipitation in the upper Indus basin with glacier mass balances and runoff,
970 Hydrol. Earth Syst. Sci., 19(11), 4673–4687, doi:10.5194/hess-19-4673-2015, 2015.

971 Jarvis PG.: Prospects for bottom-up models. In Scaling Physiological Processes: Leaf to
972 Globe. Ehleringer JR, Field CB (eds). Academic Press, 1993.

973 Jiang, H., Zheng, G., Yi, Y., Chen, D., Zhang, W., Yang, K. and Miller, C. E.: Progress and
974 Challenges in Studying Regional Permafrost in the Tibetan Plateau Using Satellite Remote
975 Sensing and Models, Front. Earth Sci., 8(December), doi:10.3389/feart.2020.560403, 2020.

976 Krogh, S. A., Pomeroy, J. W. and Marsh, P.: Diagnosis of the hydrology of a small Arctic basin
977 at the tundra-taiga transition using a physically based hydrological model, J. Hydrol.,
978 550(May), 685–703, doi:10.1016/j.jhydrol.2017.05.042, 2017.

979 Kurylyk, B. L., M. Hayashi, W. L. Quinton, J. M. McKenzie, and C. I. Voss: Influence of vertical
980 and lateral heat transfer on permafrost thaw, peatland landscape transition, and
981 groundwater flow, Water Resour. Res., 52, 1286–1305, doi:10.1002/2015WR018057, 2016.

982 Lafrenière, M. J., and Lamoureux, S. F.: Effects of changing permafrost conditions on
983 hydrological processes and fluvial fluxes. Earth-Science Reviews, 191, 212–223, 2019.

984   Li, X., Wu, T., Zhu, X., Jiang, Y., Hu, G., & Hao, J., et al.: Improving the Noah-MP model for
985   simulating hydrothermal regime of the active layer in the permafrost regions of the
986   Qinghai-Tibet Plateau. Journal of Geophysical Research: Atmospheres, 125, e2020JD032588.
987   https://doi.org/10.1029/2020JD032588, 2020

988   Lindstrom, G., Bishop, K., and Lofvenius, M. O.: Soil frost and runoff at Svartberget, northern
989   Sweden—measurements and model analysis. Hydrol. Process. 16, 3379–3392, 2002

990   Liu, Y., Zhao, L., and Li, R.: Simulation of the soil water-thermal features within the active
991   layerin Tanggula region, Tibetan plateau, by using SHAW model. J. Glaciol. Geocryol. 35,
992   280–290, 2013

993   Lyon, S. W., Destouni, G., Giesler, R., Humborg, C., Mörth, M., Seibert, J., Karlsson, J. and
994   Troch, P. A.: Estimation of permafrost thawing rates in a sub-arctic catchment using
995   recession flow analysis, Hydrol. Earth Syst. Sci., 13(5), 595–604, doi:10.5194/hess-13-595-
996   2009, 2009.

997   Ma, R., Sun, Z., Hu, Y., Chang, Q., Wang, S., Xing, W. and Ge, M.: Hydrological connectivity
998   from glaciers to rivers in the Qinghai-Tibet Plateau: Roles of suprapermafrost and
999   subpermafrost groundwater, Hydrol. Earth Syst. Sci., 21(9), 4803–4823, doi:10.5194/hess-
1000 21-4803-2017, 2017.

1001 Ma, R., Sun, Z., Chang, Q., Ge, M., Pan, Z.: Control of the interactions between stream and
1002 groundwater by permafrost and seasonal frost in an alpine catchment, northeastern Tibet
1003 Plateau, China. Journal of Geophysical Research: Atmospheres, 126, e2020JD033689, 2021

1004 McNamara, J. P., Kane, D. L. and Hinzman, L. D.: An analysis of streamflow hydrology in the
1005 Kuparuk River Basin, Arctic Alaska: A nested watershed approach, J. Hydrol., 206(1–2), 39–
1006 57, doi:10.1016/S0022-1694(98)00083-3, 1998.

1007 Muster, S., Langer, M., Heim, B., Westermann, S. and Boike, J.: Subpixel heterogeneity of ice-
1008 wedge polygonal tundra: A multi-scale analysis of land cover and evapotranspiration in the
1009 Lena River Delta, Siberia, Tellus, Ser. B Chem. Phys. Meteorol., 64(1), 0–19,
1010 doi:10.3402/tellusb.v64i0.17301, 2012.

1011 Nash, J. and Sutcliffe, J.V.: River Flow Forecasting through Conceptual Models Part I—A
1012 Discussion of Principles. Journal of Hydrology, 10, 282-290,
1013 http://dx.doi.org/10.1016/0022-1694(70)90255-6, 1970

1014 Nyberg, L.: Soil frost effects on soil water and runoff dynamics along a boreal forest
1015 transect: 1. Field investigations. Hydrol. Process. 15, 909–926, 2001.

1016 Niu, G. Y. and Yang, Z. L.: Effects of frozen soil on snowmelt runoff and soil water storage at
1017 a continental scale, J. Hydrometeorol., 7(5), 937–952, doi:10.1175/JHM538.1, 2006.

1018 Niu L, Ye B S, Li J, et al.: Effect of permafrost degradation on hydrological processes in
1019 typical basins with various permafrost coverage in Western China. Sci China Earth Sci, doi:
1020 10.1007/s11430-010-4073-1, 2010.

1021 Nitze, I., Grosse, G., Jones, B. M., Romanovsky, V. E. and Boike, J.: Remote sensing quantifies

widespread abundance of permafrost region disturbances across the Arctic and Subarctic, Nat. Commun., 9(1), 1–11, doi:10.1038/s41467-018-07663-3, 2018.

Oleson, K. and Lawrence, D.: NCAR / TN-503 + STR NCAR Technical Note July 2013 Technical Description of version 4 . 5 of the Community Land Model (CLM), (March 2014), 2013.

Osuch, M., Wawrzyniak, T. and Nawrot, A.: Diagnosis of the hydrology of a small Arctic permafrost catchment using HBV conceptual rainfall-runoff model, Hydrol. Res., 50(2), 459–478, doi:10.2166/nh.2019.031, 2019.

Pan, X., Li, Y., Yu, Q., Shi, X., Yang, D. and Roth, K.: Effects of stratified active layers on high-altitude permafrost warming: A case study on the Qinghai-Tibet Plateau, Cryosphere, 10(4), 1591–1603, doi:10.5194/tc-10-1591-2016, 2016.

Pan, X., Yu, Q., You, Y., Chun, K. P., Shi, X. and Li, Y.: Contribution of supra-permafrost discharge to thermokarst lake water balances on the northeastern Qinghai-Tibet Plateau, J. Hydrol., 555(November), 621–630, doi:10.1016/j.jhydrol.2017.10.046, 2017.

Pan, Z., Sun, Z., Hu, Y., Chang, Q., Ge, M., Wang, S., Bu, J., Long, X., Pan, Y. and Zhao, L.: Datasets for research on groundwater flow and its interactions with surface water in an alpine catchment on the northeastern Tibetan Plateau, China, , (September), 2021.

Pianosi, F. and Wagener, T.: Understanding the time-varying importance of different uncertainty sources in hydrological modelling using global sensitivity analysis, Hydrol. Process., 30(22), 3991–4003, doi:10.1002/hyp.10968, 2016.

Ran, Y., Li, X., Cheng, G., Nan, Z., Che, J., Sheng, Y., Wu, Q., Jin, H., Luo, D., Tang, Z. and Wu, X.: Mapping the permafrost stability on the Tibetan Plateau for 2005–2015, Sci. China Earth Sci., 64(1), 62–79, doi:10.1007/s11430-020-9685-3, 2021.

Ran, Y. Li, X., Cheng, G., Che, J., Aalto, J. Karjalainen, O. Hjort, J., Luoto, M., Jin, H., Obu, J., Hori, M., Yu, Q., Chang, X. (2022) New high-resolution estimates of the permafrost thermal state and hydrothermal conditions over the Northern Hemisphere. Earth System Science Data, 14, 865–884. Doi: 10.5194/essd-14-865-2022.

Romanovsky, V.E., and Osterkamp, T.E. (2000) Effects of unfrozen water on heat and mass transport processes in the active layer and permafrost. Permafrost, and Periglacial Processes. 11(3), 219-239

Savenije, H.H.G.:HESS Opinions: "The art of hydrology". Hydrol. Earth Syst. Sci., 13, 157–161, 2009

Savenije, H.H.G.: HESS Opinions "Topography driven conceptual modelling (FLEXTopo)". Hydrol. Earth Syst. Sci. 14 (12), 2681–2692. https://doi.org/10.5194/hess-14-2681-2010, 2010.

Seibert, J. and McDonnell, J. J.: On the dialog between experimentalist and modeler in catchment hydrology: Use of soft data for multicriteria model calibration, Water Resour. Res., 38(11), 23-1-23–14, doi:10.1029/2001wr000978, 2002.

Shanley, J. B. and Chalmers, A.: The effect of frozen soil on snowmelt runoff at Sleepers River, Vermont, Hydrol. Process., 13(12–13), 1843–1857, doi:10.1002/(SICI)1099-1085(199909)13:12/13<1843::AID-HYP879>3.0.CO;2-G, 1999.

Sheng, Y.: Map of permafrost distribution in the Qilian Mountains. National Tibetan Plateau Data Center, doi:10.11888/Geocry.tpdc.270456. CSTR: 18406.11.Geocry.tpdc.270456, 2020.

Sivapalan, M., Blöschl, G., Zhang, L. and Vertessy, R.: Downward approach to hydrological prediction, Hydrol. Process., 17(11), 2101–2111, doi:10.1002/hyp.1425, 2003.

Sjöberg, Y., Frampton, A. and Lyon, S. W.: Using streamflow characteristics to explore permafrost thawing in northern Swedish catchments, Hydrogeol. J., 21(1), 121–131, doi:10.1007/s10040-012-0932-5, 2013.

Sokolov, K., Fedorova, L. and Fedorov, M.: Prospecting and evaluation of underground massive ice by ground-penetrating radar, Geosci., 10(7), 1–14, doi:10.3390/geosciences10070274, 2020.

Song C, Wang G, Mao T, Dai J, Yang D. 2020. Linkage between permafrost distribution and river runoff changes across the Arctic and the Tibetan Plateau. Science China Earth Sciences, 63: 292–302

Streletskiy, D. A., Tananaev, N. I., Opel, T., Shiklomanov, N. I., Nyland, K. E., Streletskaya, I. D., Tokarev, I. and Shiklomanov, A. I.: Permafrost hydrology in changing climatic conditions: Seasonal variability of stable isotope composition in rivers in discontinuous permafrost, Environ. Res. Lett., 10(9), doi:10.1088/1748-9326/10/9/095003, 2015.

Sun, A., Quantified hydrological responses to permafrost degradation in the headwaters of the Yellow River (HWYR) in High Asia. Science of the Total Environment, 712135632 Permafrost Hydrology Research Domain: Process-Based Adjustment, 2020.

Sun, Z., Zhao, L., Hu, G., Qiao, Y., Du, E., Zou, D., et al: Modeling permafrost changes on the Qinghai-Tibetan plateau from 1966 to 2100: a case study from two boreholes along the Qinghai-Tibet engineering corridor. Permafr. Periglac. Process. 31, 156–171, doi:10.1002/ppp.2022, 2019.

Tananaev, N., Teisserenc, R. and Debolskiy, M.: Permafrost hydrology research domain: Process-based adjustment, Hydrology, 7(1), doi:10.3390/hydrology7010006, 2020.

Walvoord, M. A. and Kurylyk, B. L.: Hydrologic Impacts of Thawing Permafrost-A Review, Vadose Zo. J., 15(6), vzj2016.01.0010, doi:10.2136/vzj2016.01.0010, 2016.

Wang, G. X.,Mao, T. X., Chang, J., Song, C. L., and Huang, K. W.: Processes of runoff generation operating during the spring and autumn seasons in a permafrost catchment on semi-arid plateaus. J. Hydrol. 550, 307–317. doi:10.1016/j.jhydrol.2017.05.020, 2017.

Wang, L., Koike, T., Yang, K., Jin, R. and Li, H.: Frozen soil parameterization in a distributed biosphere hydrological model, Hydrol. Earth Syst. Sci., 14(3), 557–571, doi:10.5194/hess-14-557-2010, 2010.

Wang, P., Huang, Q., Pozdniakov, S. P., Liu, S., Ma, N., Wang, T., Zhang, Y., Yu, J., Xie, J., Fu,

G., Frolova, N. L. and Liu, C.: Potential role of permafrost thaw on increasing Siberian river discharge, Environ. Res. Lett., 16(3), doi:10.1088/1748-9326/abe326, 2021.

Wang Q F, Jin H J, Zhang T J, et al.: Active layer seasonal freeze-thaw processes and influencing factors in the alpine permafrost regions in the upper reaches of the Heihe River in Qilian Mountains (in Chinese). Chin Sci Bull, 61: 2742–2756, doi: 10.1360/N972015-01237, 2016.

Wang, T., Yang, D., Yang, Y., Piao, S., Li, X., Cheng, G. and Fu, B.: Permafrost thawing puts the frozen carbon at risk over the Tibetan Plateau, Sci. Adv., 6(19), 2–10, doi:10.1126/sciadv.aaz3513, 2020.

Wang, Y., Yang, H., Gao, B., Wang, T., Qin, Y. and Yang, D.: State Key Laboratory of Hydroscience and Engineering , Department of Hydraulic School of Water Resources and Environment , China University of Geosciences , 2018.

Watson, V., Kooi, H. and Bense, V.: Potential controls on cold-season river flow behavior in subarctic river basins of Siberia, J. Hydrol., 489, 214–226, doi:10.1016/j.jhydrol.2013.03.011, 2013.

Woo, M-K.: Permafrost Hydrology, Springer, 5, 2012.

Wu, T., Li, S., Cheng, G. and Nan, Z.: Using ground-penetrating radar to detect permafrost degradation in the northern limit of permafrost on the Tibetan Plateau, Cold Reg. Sci. Technol., 41(3), 211–219, doi:10.1016/j.coldregions.2004.10.006, 2005.

Xiao, Y., Zhao, L., Dai, Y., Li, R., Pang, Q. and Yao, J.: Representing permafrost properties in CoLM for the Qinghai-Xizang (Tibetan) Plateau, Cold Reg. Sci. Technol., 87, 68–77, doi:10.1016/j.coldregions.2012.12.004, 2013.

Xie, C., Gough, W.A.: Short Communication: A Simple Thaw-Freeze Algorithm for a Multi-Layered Soil using the Stefan Equation. Permafrost and Periglac. Process. 24: 252–260, 2013.

Yang, Y., Wu, Q., Jin, H., Wang, Q., Huang, Y., Luo, D., Gao, S. and Jin, X.: Delineating the hydrological processes and hydraulic connectivities under permafrost degradation on Northeastern Qinghai-Tibet Plateau, China, J. Hydrol., 569(November 2018), 359–372, doi:10.1016/j.jhydrol.2018.11.068, 2019.

Ye, B., Yang, D., Zhang, Z. and Kane, D. L.: Variation of hydrological regime with permafrost coverage over Lena Basin in Siberia, J. Geophys. Res. Atmos., 114(7), doi:10.1029/2008JD010537, 2009.

Zhang, R., Liu, J., Gao, H. and Mao, G.: Can multi-objective calibration of streamflow guarantee better hydrological model accuracy?, J. Hydroinformatics, 20(3), 687–698, doi:10.2166/hydro.2018.131, 2018.

Zhang, T., Frauenfeld, O. W., Serreze, M. C., Etringer, A., Oelke, C., McCreight, J., Barry, R. G., Gilichinsky, D., Yang, D., Ye, H., Ling, F. and Chudinova, S.: Spatial and temporal variability in active layer thickness over the Russian Arctic drainage basin, J. Geophys. Res. D Atmos., 110(16), 1–14, doi:10.1029/2004JD005642, 2005.

1136 Zhang, X. : High-resolution precipitation data derived from dynamical downscaling using
1137 the WRF model for the Heihe River Basin, northwest China. Theor Appl Climatol, 131:1249–
1138 1259, 2018.

1139 Zhao, L., Zou, D., Hu, G., Du, E., Pang, Q., Xiao, Y., Li, R., Sheng, Y., Wu, X., Sun, Z., Wang, L.,
1140 Wang, C., Ma, L., Zhou, H. and Liu, S.: Changing climate and the permafrost environment on
1141 the Qinghai–Tibet (Xizang) plateau, Permafr. Periglac. Process., 31(3), 396–405,
1142 doi:10.1002/ppp.2056, 2020.

1143 Zhou, J., Kinzelbach, W., Cheng, G., Zhang, W., He, X. and Ye, B.: Monitoring and modeling
1144 the influence of snow pack and organic soil on a permafrost active layer, qinghai-tibetan
1145 plateau of china, Cold Reg. Sci. Technol., 90–91, 38–52,
1146 doi:10.1016/j.coldregions.2013.03.003, 2013.

1147 Zou, D., Zhao, L., Wu, T., Wu, X., Pang, Q. and Wang, Z.: Modeling ground surface
1148 temperature by means of remote sensing data in high-altitude areas: test in the central
1149 Tibetan Plateau with application of moderate-resolution imaging spectroradiometer
1150 Terra/Aqua land surface temperature and ground-based infrared, J. Appl. Remote Sens.,
1151 8(1), 083516, doi:10.1117/1.jrs.8.083516, 2014.

1152

1153 # Tables

1154 Table 1. The water balance and constitutive equations used in FLEX-Topo-FS model. In Equation
1155 10, 11, and 12, the S_u and S_{umax} represent root zone reservoirs and their storage capacities in
1156 different landscapes, including vegetation hillslope (S_{umax_V}), alpine desert (S_{umax_D}) and riparian
1157 (S_{umax_R}).

reservoirs	Water balance equations	Constitutive equations
Snow reservoir	$\dfrac{dS_w}{dt} = P - M_w \ (4)$	$P_s = \begin{cases} 0; & T > 0 \\ P; & T \le 0 \end{cases} \ (5)$
		$M_w = \begin{cases} F_{dd} \cdot T; & T > 0 \\ 0; & T \le 0 \end{cases} \ (6)$
Glacier reservoir	$\dfrac{dS_g}{dt} = P_l + M_g - Q_g \ (7)$	$M_g = \begin{cases} F_{dd} \cdot T \cdot C_g; & S_w = 0 \text{ and } T > 0 \\ 0; & S_w > 0 \text{ or } T \le 0 \end{cases} \ (8)$
		$Q_g = S_g / K_f \ (9)$

Root zone reservoir	$\dfrac{\mathrm{d}\,S_{\mathrm{u}}}{\mathrm{d}t} = P_l + M_w - E_a - R_{\mathrm{u}}$ (10)	$R_{\mathrm{u}} = (P_l + M_w)\cdot(1 - (1 - \dfrac{S_{\mathrm{u}}}{S_{\mathrm{umax}}})^{\beta})$ (11)

$$E_a = E_p \cdot (\dfrac{S_u}{C_e \cdot S_{u\,\max}})\ \ (12)$$

Splitter and lag function		$R_f = R_u D$ (13); $R_s = R_u(1 - D)$ (14)

$$R_{fl}(t) = \sum_{i=1}^{T_{lagf}} c_f(i)\cdot R_f(t - i + 1)\ (15)$$

$$c_f(i) = i / \sum_{u=1}^{T_{lagf}} u\ (16)$$

Fast reservoir	$\dfrac{\mathrm{d}\,S_{\mathrm{f}}}{\mathrm{d}t} = R_{\mathrm{f}} - Q_{\mathrm{f}}$ (17)	$Q_f = S_f / K_f$ (18)

1158

1159 Table 2. The parameters of the FLEX-Topo-FS model, and their prior ranges for calibration.

Parameter	Explanation	Prior range for calibration
$F_{\mathrm{dd}}(\mathrm{mm}\cdot{}^{\circ}\mathrm{C}^{-1}\cdot\mathrm{d}^{-1})$	snow degree-day factor	(1-5)
C_{g} (-)	Glacier degree-factor multiplier	(1-3)
$S_{\mathrm{umax\_V}}$ (mm)	Root zone storage capacity for vegetation hillslope	(50, 200)
$S_{\mathrm{umax\_D}}$ (mm)	Root zone storage capacity for alpine desert	(10, 100)
$S_{\mathrm{umax\_R}}$ (mm)	Root zone storage capacity for riparian	(10, 100)
β (-)	The shape of the storage capacity curve	(0, 1)
C_e (-)	Soil moisture threshold for reduction of evaporation	(0.1, 1)
D (-)	Splitter to fast and slow response reservoirs	0.2
T_{lagF} (days)	Lag time from rainfall to peak flow	(0.8, 3)

K_f (days)	fast recession coefficient	(1, 10)
K_s (days)	baseflow recession coefficient	(10, 100)
k (W/(m·K))	thermal conductivity	2
ω (-)	water content, as a decimal fraction of the dry soil weight	0.12
ρ (kg/m^3)	bulk density of the soil	1000

1160

1161 **Figures**

1162
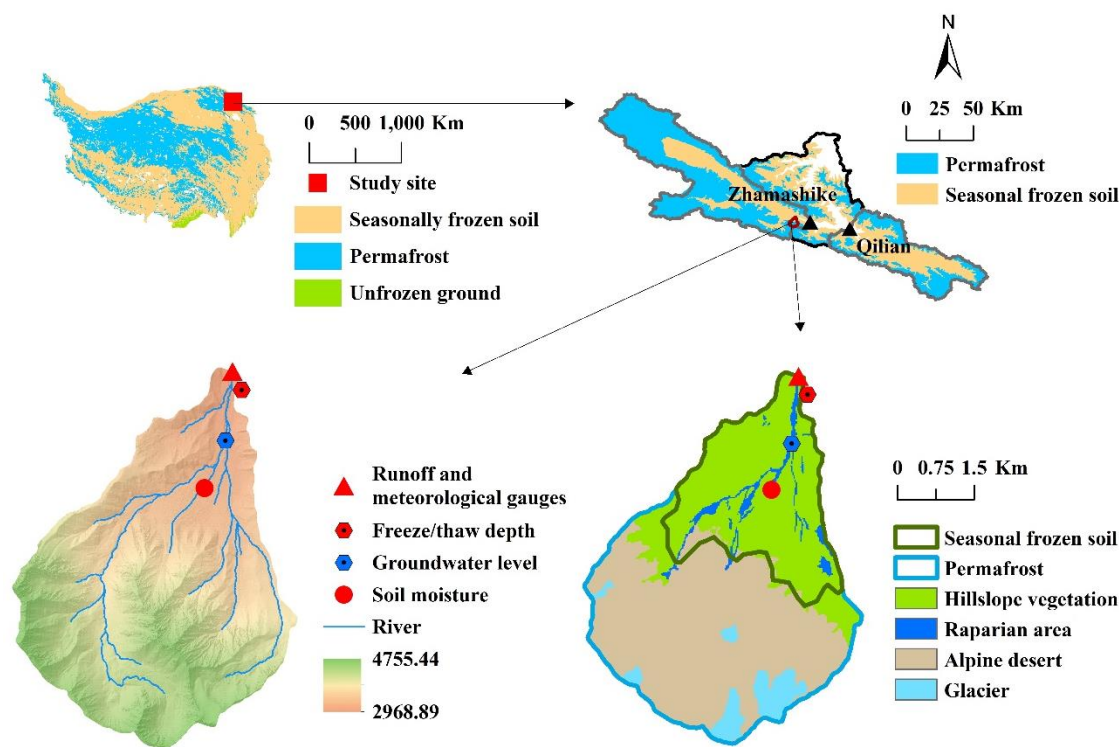
1163 Figure 1. Sketch map of the Qinghai-Tibetan Plateau, and the distribution of permafrost and
1164 seasonal frozen-soil of the ~~Tibetan Plateau~~QTP (Zou et al., 2014), and the location of the
1165 upper Heihe River basin (up left); sketch map of permafrost and seasonal frozen-soil
1166 distribution of the upper Heihe river basin (Sheng, 2020), and the two sub-basins, i.e.
1167 Zhamashike and Qilian, and the location of the Hulu catchment (up right); Hulu catchment's
1168 digital elevation model (DEM), river channel, runoff and meteorological gauge station
1169 (observed from 2011 to 2014), the locations for soil moisture (2011-2013 with data gap),
1170 groundwater level (2016-2019), and freeze/thaw depth (bottom left) (2011-2014);
1171 landscapes and seasonal frozen-soil / permafrost map of the Hulu catchment (bottom
1172 right).

1173
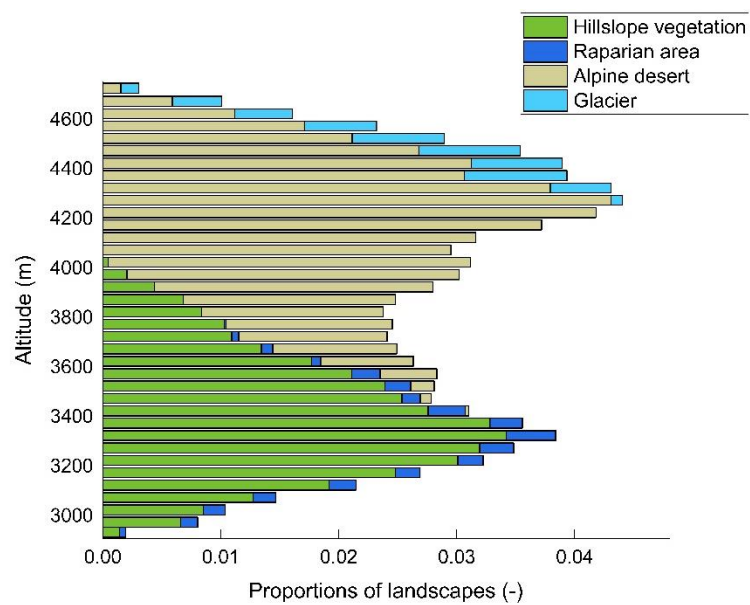
1174

1175   Figure 2. Landscape classification at different elevation bands (with 50m interval) of the Hulu
1176   catchment.

1177
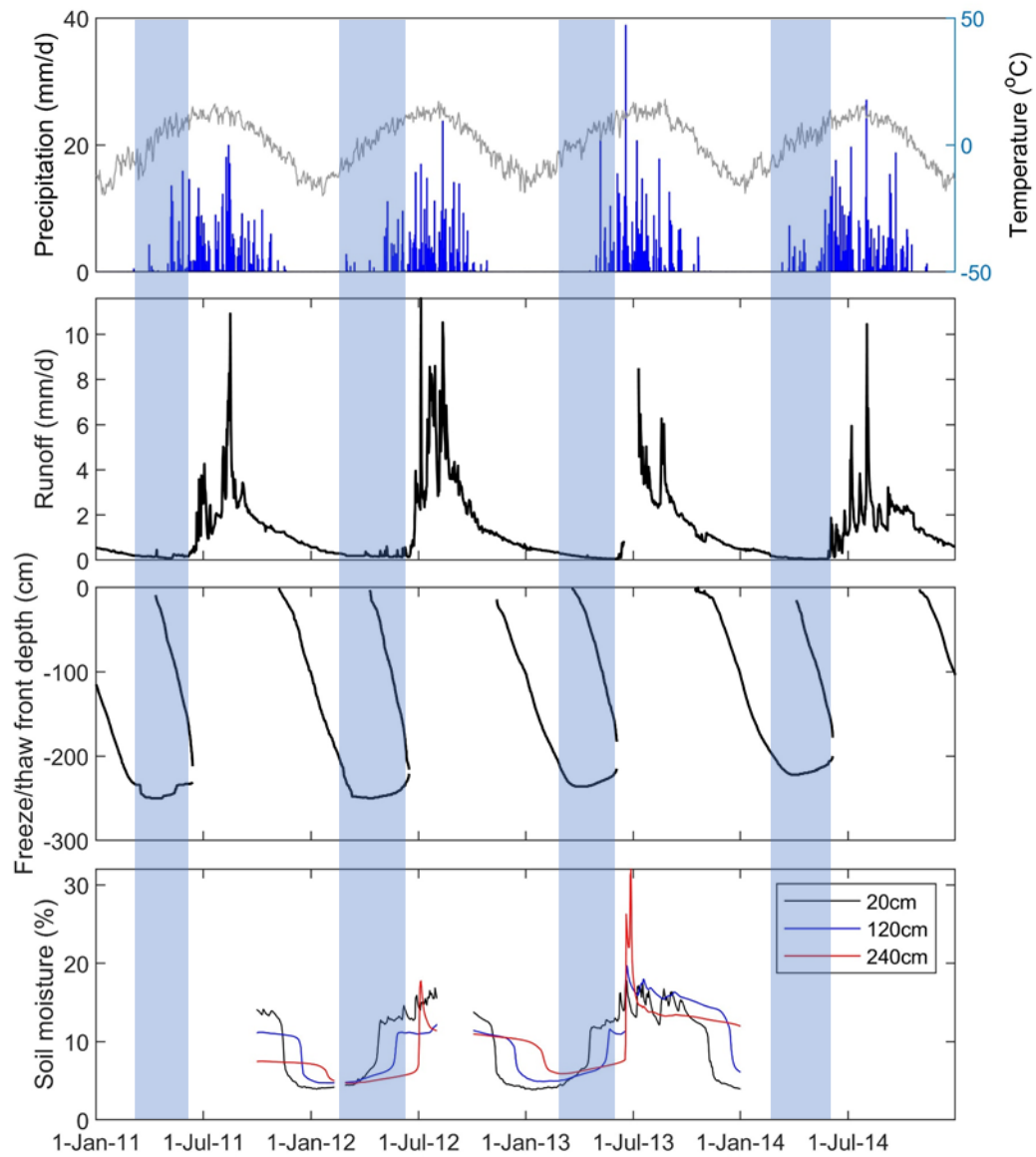
1178 Fig 3. Observed daily precipitation and air temperature; observed daily runoff depth of the
1179 Hulu catchment; observed freeze/thaw front depth; observed soil moisture at the depth of
1180 20cm, 120cm, 240cm.

1181
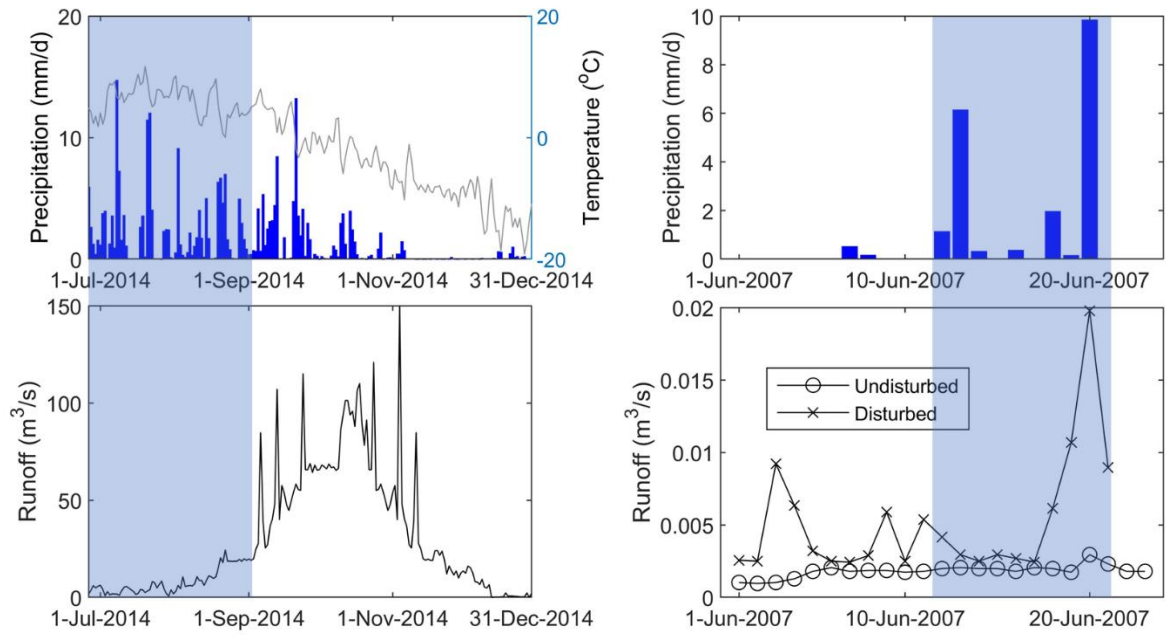
1182 Fig 4. The Little-Runoff in the Early Thawing season (LRET) phenomenon in other places, e.g.

1183 the headwater of Yellow River (Yang et al., 2019), and athe small headwater catchment at

1184 Cape Bounty Arctic Watershed Observatory, Melville Island, NU in Canada (Lafrenière and

1185 Lamoureux, 2019)

1186

1187
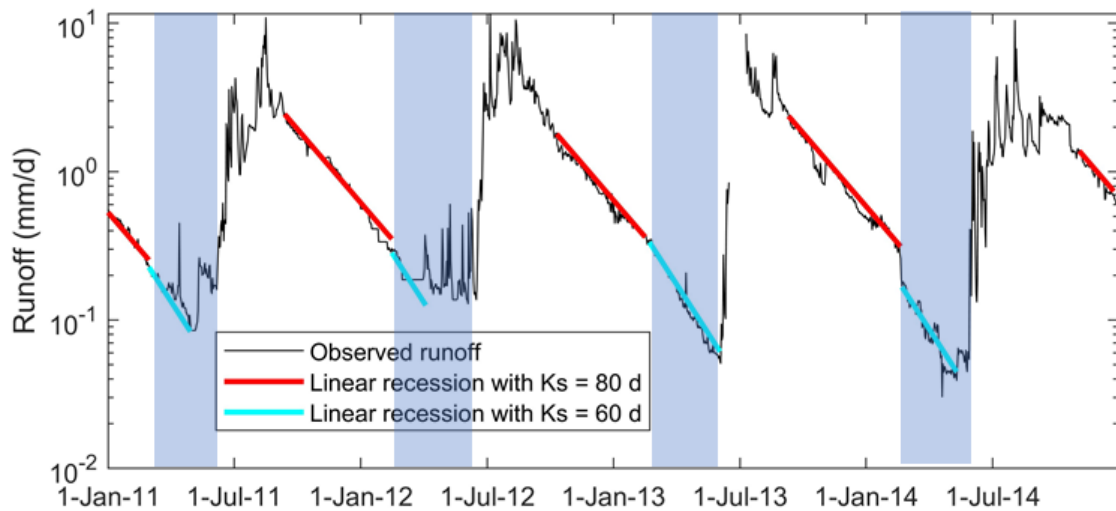
1188 Figure 5. Groundwater recession, from 2011 to 2014, on logarithmic scale, with linear

1189 recession parameter K_s = 80 d in the early recession periods and K_s = 60 d in the end of

1190 recession periods.

1191
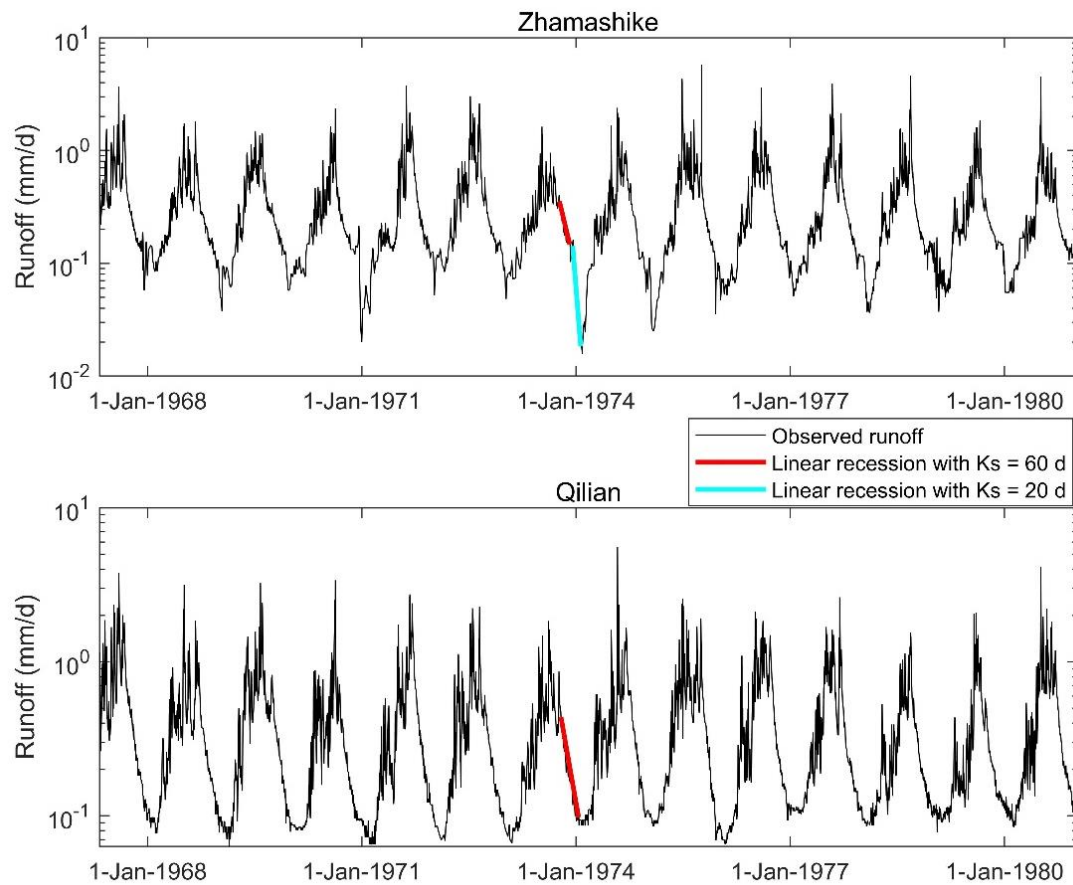
1192   Figure 6. The hydrograph of the Zhamashike and Qilian sub-basin on logarithmic scale, and
1193   the linear recession curve with K_s = 60d and K_s =20d.

1194
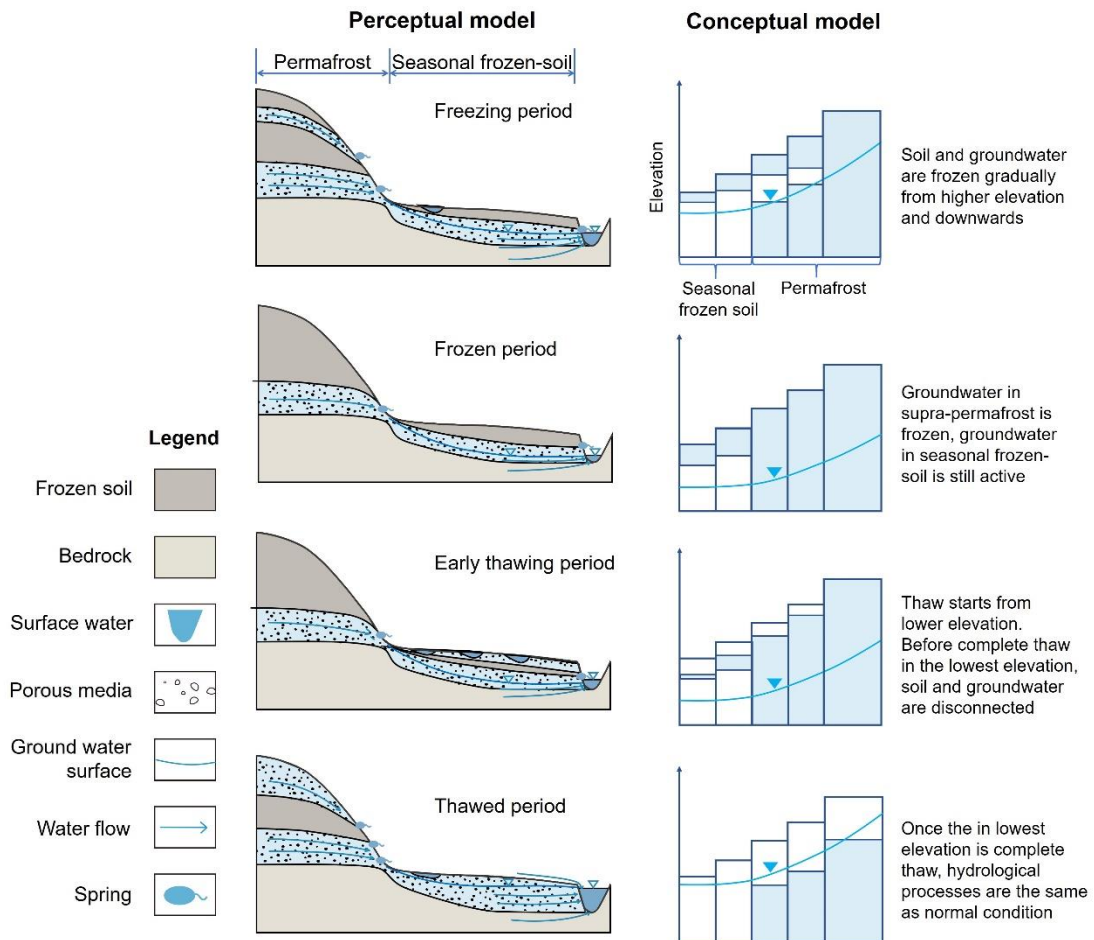
1195   Figure 7 The perceptual and conceptual FLEX-Topo-FS frozen-soil hydrological models.

1196
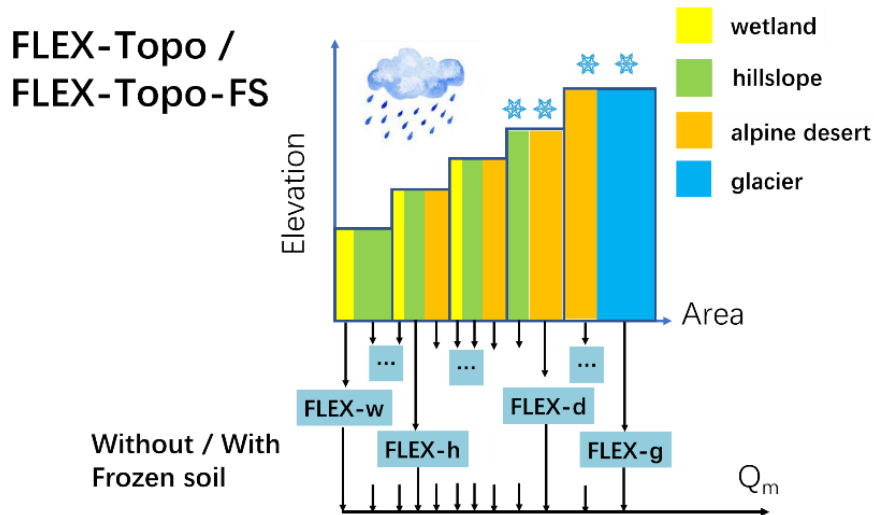
1197   Fig 8. Model structures of FLEX-Topo, and FLEX-Topo-FS. FLEX-w means the module for
1198   wetland, FLEX-h for hillslope, FLEX-d for alpine desert, and FLEX-g for glacier, respectively.

1199

1200

1202

1203 Fig 109. Comparison between simulated freeze/thaw depth by Stefan equation and
1204 observation.

1205

1206
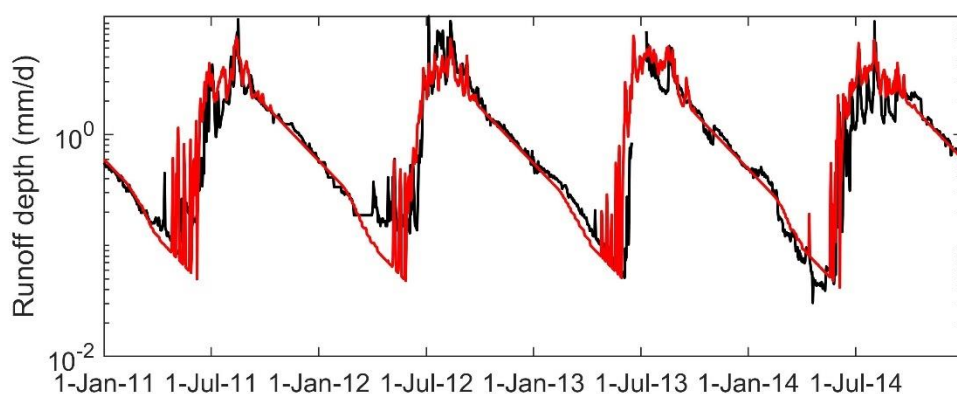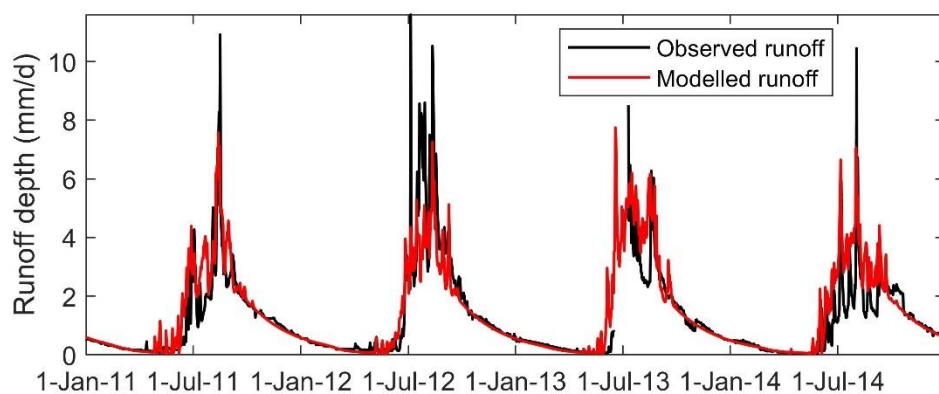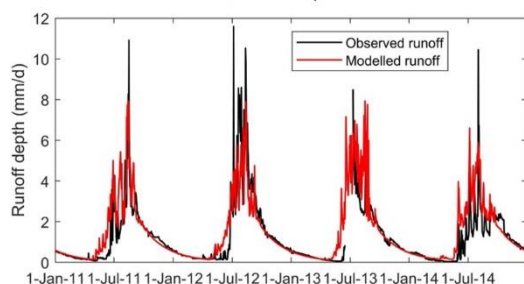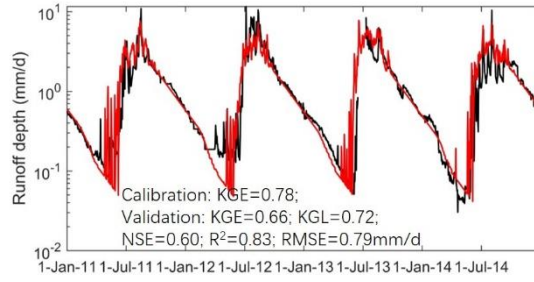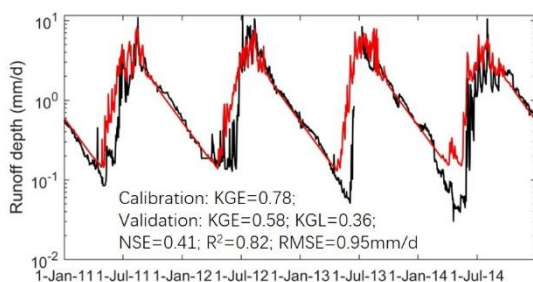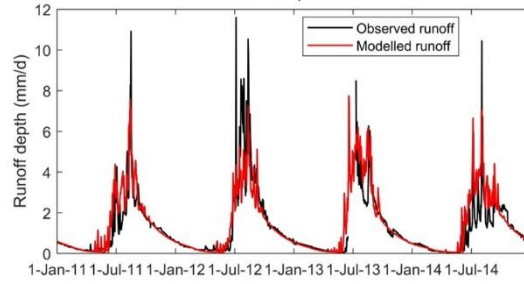
1207 Figure 1~~0~~1. Modeling results of FLEX-Topo and FLEX-Topo-FS models, and the
1208 comparisons with observation, on both normal and logarithm scales. ~~Modeling results of~~

1211
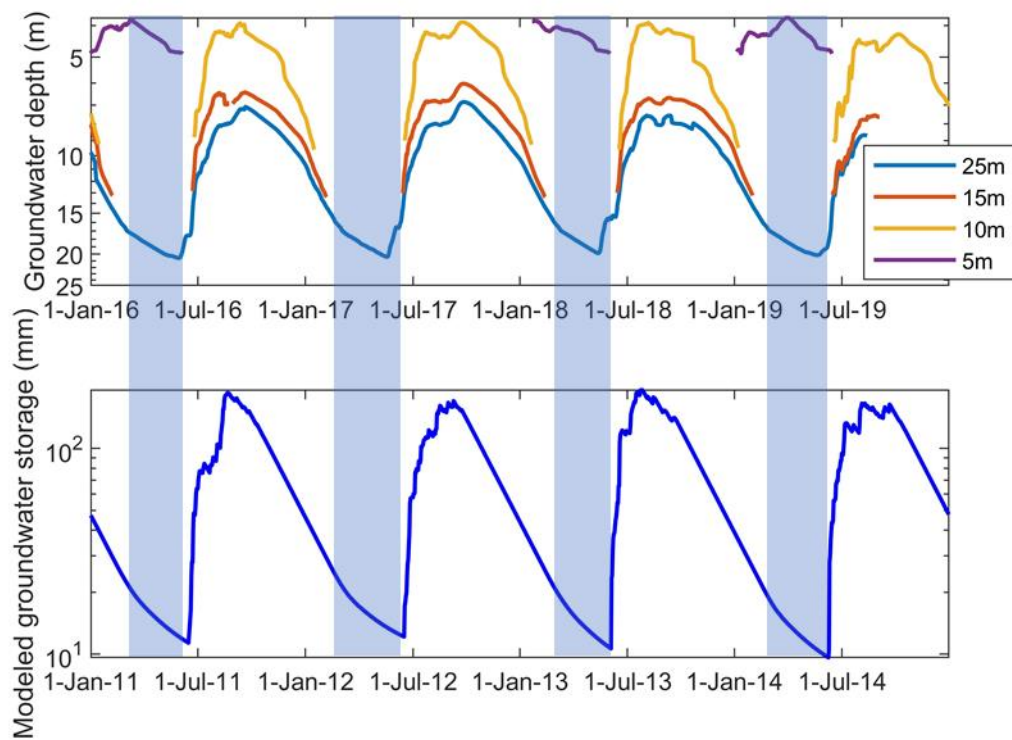
1212   Figure 112. Observed groundwater depth from 2016 to 2019 at WW01 wells at depth of 5m,
1213   10m, 15m, and 25m. And the simulated groundwater storage by the FLEX-Topo-FS model
1214   from 2011 to 2014.
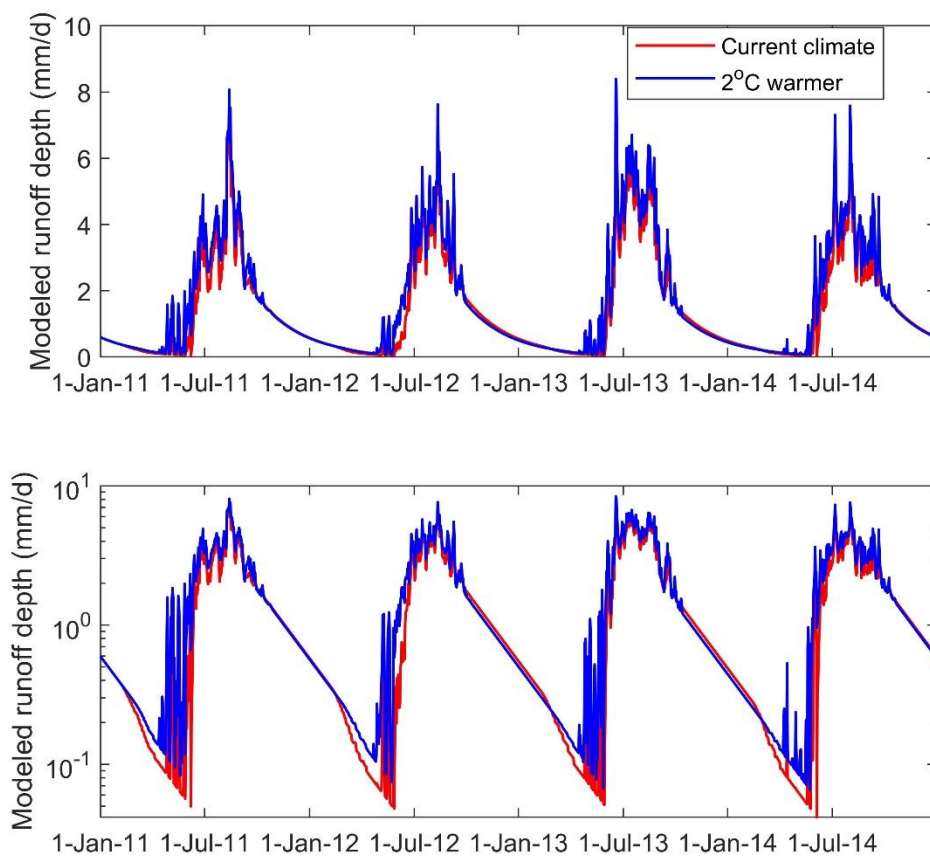
1215

1216   Figure ~~13~~12. Simulated hydrograph in current climate condition, and the 2°C warmer

1217   condition.